Integrated Terrestrial-Wired and LEO Satellite With Offline Bidirectional Cooperation for 6G IoT Networks

Ashfaq Ahmed, *Senior Member, IEEE*, Arafat Al-Dweik, *Senior Member, IEEE*, Youssef Iraqi, *Senior Member, IEEE*, and Ernesto Damiani, *Senior Member, IEEE*

***Abstract*—This article presents a novel framework for integrating low-Earth orbit satellites (LEOSs) with terrestrial-wired networks to improve coverage, throughput, and transmission reliability of sixth generation (6G) Internet of Things (IoT) networks. The proposed framework utilizes the synergy of nonorthogonal multiple access (NOMA), automatic repeat request (ARQ), and cooperative communications to maximize the data downloaded from a LEOS to multiple terrestrial users. More specifically, we propose a novel offline packets repair and recovery (PRR) technique to reduce the number of dropped packets, where the wired-terrestrial connection is used to enable efficient bidirectional cooperation, to improve the reliability of the received data by reducing the multiuser interference inherent to NOMA. Moreover, by exchanging the acknowledgment messages used with ARQ, efficient chase combining (CC) is applied to improve the signal to noise ratio (SNR) of the received packets. Extensive Monte Carlo simulation experiments are used to evaluate and quantify the advantages of the proposed system. The results obtained show that the proposed system can repair a significant number of dropped packets, which reduces the packet drop rate and improves the network throughput. In several scenarios, the proposed PRR managed to repair and recover more than 90% of the dropped packets.**

***Index Terms*—Automatic repeat request (ARQ), chase combining (CC), maximum ratio combining (MRC), nonorthogonal multiple access (NOMA), packet drop rate (PDR), sixth generation (6G), throughput.**

I. Introduction

THE ADVENT of revolutionary wireless applications in the past decade has outlined the need for ubiquitous connectivity and computing for cutting-edge technologies. These novel technologies include holographic applications, telemedicine, massive machine-type communications, and autonomous systems [1], [2], where Internet of Things (IoT) is the core of these applications [2]. The increasing number of new subscribers, high-data rate systems, and IoT applications have significantly increased the demand for data access during the recent past. According to the Ericsson Mobility Report [3], mobile network data traffic increased by 44% in a single year between 2020 and 2021. This data traffic volume has surpassed 72 exabyte and is generated by approximately 8 billion subscribers. Furthermore, CISCO indicated that, by 2023, half of IoT devices will be incorporated into existing cellular networks [4]. Consequently, it is expected that wireless networks will need to accommodate 15 billion IoT devices in addition to the 8 billion existing mobile users.

Although fifth generation (5G) networks offer significant improvements over fourth generation (4G), its capacity enhancement still lags behind the 1000-fold increase predicted by the international mobile telecommunications (IMT)-2020 vision. Therefore, the wireless communications ecosystem foresees that satellite communications will be pivotal for beyond 5G and sixth generation (6G) wireless networks. Moreover, Third Generation Partnership Project (3GPP) has already started to discuss integrating satellite communications with 5G networks, which is denoted as nonterrestrial network (NTN) [5]. Releases 14 to 16 consider various NTN basic issues and potential use cases such as IoT. The IoT-NTN integration was approved in Release 17. Furthermore, new radio (NR) will be supported by regenerative and transparent satellites in Releases 17 to 19 while 6G NTN will start in Release 20. NTN with a highly dense low-Earth orbit satellite (LEOS) constellation is expected to be an essential element in 6G networks [5]. It is worth noting that the 6G IoT networks still do not have a unique system design, however LEOSs and unmanned aerial vehicles (UAVs) are visioned to be fundamental elements in such networks [6].

Nonorthogonal multiple access (NOMA) has gained huge attention in recent years as a potential technique for future mobile networks due to its intrinsic ability to provide high-spectral efficiency, massive connectivity, and low latency [7], [8], [9], [10], [11], [12]. Furthermore, the performance gains of integrating NOMA with various applications, such as IoT, short packet communication (SPC), satellite communications, UAV communications, visible light communication (VLC), underwater communications, intelligent reflecting surface (IRS) communications, and cooperative communications, are being widely investigated [13], [14], [15], [16], [17]. Power domain (PD) or code

Manuscript received 2 November 2023; revised 4 December 2023; accepted 28 December 2023. Date of publication 1 January 2024; date of current version 25 April 2024. *(Corresponding author: Arafat Al-Dweik.)*

Ashfaq Ahmed and Ernesto Damiani are with the Center for Cyber Physical Systems, Department of Computer and Communication Engineering, Khalifa University, Abu Dhabi, UAE (e-mail: ashfaq.ahmed@ku.ac.ae; ernesto.damiani@ku.ac.ae).

Arafat Al-Dweik is with the 6G Research Center, Department of Computer and Communication Engineering, Khalifa University, Abu Dhabi, UAE (e-mail: dweik@fulbrightmail.org).

Youssef Iraqi is with the College of Computing, University Mohammed VI Polytechnic, Ben Guerir 43150, Morocco (e-mail: youssef.iraqi@um6p.ma).

Digital Object Identifier 10.1109/JIOT.2023.3349144

domain (CD) NOMA enable data transfer to multiple users simultaneously. The total available power is shared among users in the PD-NOMA, where the user with the weakest channel is assigned the maximum power and the user with the best channel is assigned the least power. Although the ultimate performance of NOMA can be obtained using adaptive power assignment [18], fixed power assignment is adopted to reduce the complexity of the system and signaling overhead. The transmitter uses the superposition coding (SC) technique to generate the NOMA signal. Each user receives the NOMA signal and applies the successive interference cancellation (SIC) process to detect its own signal, except for the user with the highest power, who can detect its own signal directly. Although NOMA is a spectrum-efficient technology capable of meeting some of the requirements of ubiquitous connectivity, power sharing between users can harm each user's reliable data delivery.

Automatic repeat request (ARQ) is considered one of the main technologies to provide guaranteed Quality of Service (QoS) for wireless systems. Therefore, it has been adopted in most commercial wireless communications standards. For example, it has been adopted for long term evolution (LTE) networks [19]. The Radio Link Control sublayer [20] uses ARQ while hybrid-ARQ (HARQ) is used by the medium access control (MAC) [21] and Physical [22] layers. ARQ is also used in 5G networks, but it is an improved and more flexible version of ARQ in LTE. More specifically, the ARQ in 5G is adaptive and asynchronous for both the downlink and the uplink. A user equipment (UE) can support up to 16 HARQ processes if needed. Other standards that integrate ARQ include the Wireless Regional Area Networks standard (IEEE 802.22), the Wireless Local Area Networks standard (IEEE 802.11) [23], Wireless Personal Area Networks (Bluetooth) [24], IEEE 802.15.4 standard for Low-Rate Wireless Personal Area Networks [25], and many others. ARQ is also used by several nonstandardized systems, such as the NASA nano-LEOS project [26]. Standardization of NOMA is not as mature as ARQ, however, enormous attention is devoted to the inclusion of NOMA in the main standardization activities of 3GPP. A detailed discussion of the NOMA standardization efforts is given in [27].

In orthogonal multiple access (OMA), the benefit of ARQ is mainly related to the time diversity caused by multiple transmissions of the same packet at different times. If the time elapsed between multiple transmissions is longer than the channel coherence time, the channel fading gains over the multiple retransmitted packets become independent and the achieved diversity order becomes equal to the number of retransmissions performed per packet [28]. When NOMA and ARQ are integrated, the diversity advantage of ARQ is diluted because not all retransmissions can be combined [28]. Consequently, alternative techniques are required to improve the reliability of the packet detection process.

A. Related Work

Numerous research works have investigated cooperative satellite communications. For example, Zhang et al. [29] described a hybrid satellite-terrestrial IoT network. An auction-based optimization problem is proposed to maximize the sum rate of all primary receivers with the optimal secondary network selection and radio resource allocation profile while fulfilling the QoS of secondary receivers. In [30], a hybrid satellite-terrestrial spectrum sharing system is proposed where a secondary terrestrial network (TN) cooperates with a primary satellite network to increase spectral efficiency. For massive connection design, NOMA is used to establish a cognitive radio-based satellite-terrestrial system that relies on NOMA to gain even more benefits than conventional schemes. An integrated satellite/terrestrial cache-enabled radio access network (RAN) is presented in [31], in which several access points (APs) and a LEOS network serve users cooperatively. Nguyen et al. [32] investigated a hybrid satellite-terrestrial relay network that uses a number of secondary terrestrial users to share spectrum with a main satellite network to increase spectrum efficiency. In [33], the performance of a NOMA-assisted underlay cognitive hybrid satellite-TN is investigated, which consists of a primary satellite source with numerous terrestrial primary receivers and a secondary transmitter with prepaired users placed on the ground. An integrated NOMA and network-coding scheme is proposed and incorporated into a hybrid satellite-TN in [34]. The network consists of a LEOS belonging to a LEOS constellation, a base station (BS), and several mobile terminals on the ground. Yan et al. [35] investigated the outage probability and ergodic capacity of a downlink hybrid satellite-terrestrial relay network with cooperative NOMA (C-NOMA), in which the user with the strongest channel conditions serves as a relay node and forwards information to other users.

The integrated satellite-TN with C-NOMA has been widely considered in the literature. For example, the work in [36] proposed a network with a single relay, and due to its position, the near user may act as another relay that forwards satellite-sent data to the weak user. The work in [37] generally considers the same configuration [36] in but with multiple relays. The work in [38] considers that the relay performs amplify-and-forward (AF) using multiple antennas. The impact of hardware impairments is considered in [39]. The system presented in [40] analyses the outage of a network where one user can directly receive the signal from the LEOS while the other can only receive it through a demodulated-and-forward (DF) multiantenna relay. Outage probability of an AF single-antenna relay with NOMA is considered where the users are equipped with multiple antennas [41].

Li et al. [42] investigated the outage of a satellite-assisted NOMA with coordinated direct and relay transmission. In [43], an uplink Internet of remote things-focused satellite-terrestrial relay network is proposed where the far user communicates with the satellite through relays, where the relays establish communications of multiple users using the PD NOMA. In [44], a space-air-ground downlink relay system is discussed, in which the UAV serves as a relay and transmits the information acquired from satellites to ground users using NOMA. A NOMA-based satellite-TN with optimum relay selection is studied in [45] and [46] with imperfect SIC assumption and in a spectrum sharing scenario, respectively.

In [47], the performance of a NOMA-based overlay cognitive integrated satellite-terrestrial relay network is investigated with secondary network selection, where the selected secondary network accesses the licensed spectrum by assisting the primary network communication with the AF protocol. Nguyen et al. [48] investigated a satellite-terrestrial relay system that uses small-cell transmission under interference constraints with macrocell users. Furthermore, NOMA is used to enhance the spectrum efficiency. In [49], a notion of cache-enabled relays is introduced, in which the satellite pushes popular content to the relays using the NOMA protocol. Users can obtain data from relays rather than from the satellite, substantially reducing the satellite traffic. In [50], a hybrid satellite-terrestrial relay network is proposed where a satellite relays information to terrestrial users. To establish communication, a dedicated half duplex (HD)-AF relay is utilized.

An et al. [51] proposed a secured transmission scheme for an integrated LEOS and TN. By considering the mutual interference between the two networks, an optimization problem is formulated to maximize the instantaneous rate of the terrestrial user while meeting the interference constraint of the satellite user. The performance is evaluated in terms of the average secrecy rate and secrecy outage probability. Lin et al. [52] examined joint beamforming design and optimization for hybrid satellite-terrestrial relay networks in which the links between the satellite and a macro base station (MBS) to multiple users are blocked. To enhance the desired satellite signal strength at the blocked users, a refracting IRS is employed in cooperation with a MBS that functions as a decode and forward relay. The primary objective of the work is to reduce the total transmit power of both the satellite and MBS while ensuring that the rate requirements are met. Lin et al. [53] investigated hybrid beamforming schemes that are secrecy-energy efficient for a satellite-terrestrial integrated network. In this system, a multibeam satellite and a cellular network share the same spectrum. Taking into account system imperfections, the hybrid beamformer at the BS and the beamformers at the satellite were jointly designed to maximize the achievable efficiency of secrecy-energy while still meeting the signal to interference plus noise ratio (SINR) requirements of the users of both networks. Lin et al. [54] investigated the multicast communication of a satellite and aerial-integrated network with rate-splitting multiple access (RSMA). The satellite and UAV transmit at the same frequency. The UAV adopts the RSMA to provide access to the IoT and achieve the desired performance in terms of interference suppression, spectral efficiency, and hardware complexity. As can be noted from [51], [52], [53], and [54], the cooperation between terrestrial users is not considered. Furthermore, while ARQ is widely adopted in many wireless standards, its functionality and full potential with NOMA have yet to be thoroughly investigated.

B. Motivation

Ground-based BSs are often incapable of transmitting data to distant and remote users, as in the case of rural areas. To serve such unreachable users, several researchers have explored various solutions where LEOSs are considered the most viable. The effectiveness of LEOSs is due to their ability to have a line-of-sight signal component with ground users. Furthermore, due to their mobility, LEOSs can provide data access services to a large number of ground users at different geographical locations [55]. Despite the advantages of LEOSs, they have limited onboard processing capabilities, data rates, and short-time connectivity with ground users, usually only a few minutes per orbital pass. Combining NOMA, ARQ, and TNs has been proposed to improve link coverage, reliability, and throughput, but these technologies have not been used to their full potential. For instance, ARQ is only used to enhance the signal to noise ratio (SNR) during the satellite's brief flyover, without taking into account the correlation of NOMA packets caused by ARQ, or the difficulty of combining NOMA packets when the data of one user changes over the retransmissions of the other user. To address these issues, this work proposes a novel approach, called packets repair and recovery (PRR), to make use of the packet correlation inherent in the integrated ARQ, NOMA, LEOS, and TN architecture. This approach is based on three new concepts: 1) efficient NOMA combining; 2) local retroactive SIC (L-RSIC) and cooperative retroactive SIC (C-RSIC); and 3) bidirectional C-NOMA. The PRR is used to repair and recover dropped packets after they reach their maximum retransmission limit. The proposed C-NOMA is distinct from C-NOMA in that it is bidirectional and can be in the form of acknowledgment (ACK)/negative acknowledgment (NACK) messages, or the hard bits of a particular user, which are sent only when necessary to increase system efficiency.

C. Contributions

The following are the main contributions of this work.

1) Proposes a novel framework for PRR in integrated LEOSs, NOMA, ARQ, and TNs. The proposed PRR scheme allows efficient application of chase combining (CC) to NOMA by exchanging the ACK/NACK messages of both users. Therefore, the cooperation is bidirectional and limited to one bit per message.
2) Exploits the packets' correlation due to ARQ to apply retroactive SIC (RSIC) to repair and recover dropped packets offline after the satellite flyover is completed. Therefore, the satellite link throughput can be improved without the need for excessive retransmissions or cooperation with other users. The RSIC can be performed using data stored locally at each user, and hence it is termed L-RSIC.
3) In the event that CC and L-RSIC fail, the decoded bits for each user can be forwarded to the other user to enable interference cancelation, and hence enable more reliable SIC and CC. The SIC in this case is termed C-RSIC.
4) The performance of the proposed framework is evaluated in terms of packet drop rate (PDR), number of packets successfully recovered, and the throughput achieved by both users. The results show that the proposed technique can significantly reduce the PDR.

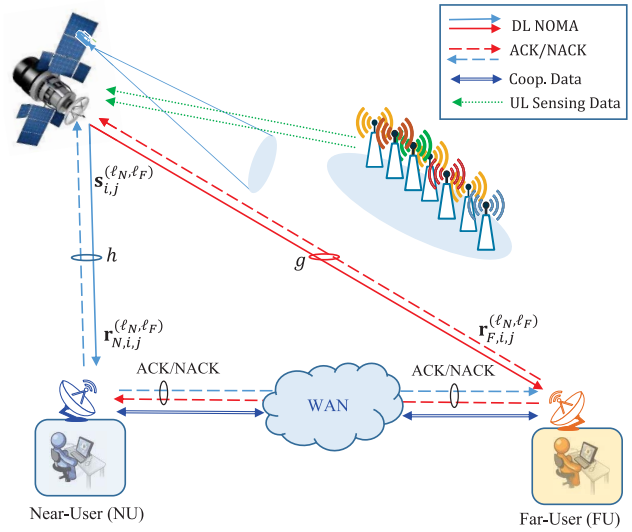

Fig. 1. Illustrative example for the DL NOMA from LEOS to ground users (solid right arrows), cooperative data between ground users (double-sided double-line arrows), uplink for IoT devices to LEOS (left dotted arrows), and bidirectional ACK/NACK (right/left dashed arrows).

5) The proposed framework is compared with the conventional C-NOMA in which the near-user (NU) decodes and forwards the far-user (FU) packet during each transmission slot (TS). The FU then combines the packet received from the LEOS and NU. The comparison results show that the proposed scheme outperforms C-NOMA using fewer packet exchanges.

D. Paper Organization

The system architecture and channel model are described in Section II. An overview of the NOMA receiver design is provided in Section III. The proposed PRR is detailed in Section IV, which includes the components of the proposed system and the practical considerations of the proposed model. Numerical results and the corresponding discussion are outlined in Section V. Finally, this work is concluded in Section VI.

II. System Architecture and Channel Model

This work considers an IoT network similar to the one shown in Fig. 1, which consists of a LEOS, two ground users, and multiple IoT nodes. The LEOS may collect data from the distributed IoT nodes, and can also generate data itself by capturing images and videos of certain phenomena, and then the LEOS downloads the collected data to the ground users. The LEOS and IoT nodes communicate through wireless links, while ground users are assumed to be separated by a large distance and therefore cannot have a direct wireless link. Consequently, they can communicate with each other only through a terrestrial wired wide area network (WAN). Wired links can provide guaranteed QoS beyond the ultra reliable low-latency communicationss (URLLCs) specifications of the 5G, particularly when the link is dedicated to the ground users as in the case of fiber leased-lines [56]. Future 6G networks might be able to support the desired QoS as they are expected to provide one tenth of the 5G latency and support dedicated links [57]. The type of data that ground users communicate is described in the following sections. The main objective of this configuration is to improve the LEOS downlink during the satellite flyover using the powerful communications resources of the TN-WAN. Therefore, in the context of this work, the satellite link utilizes TN to improve its performance while the TN does not use the LEOS link as part of its transmission links. In this work we consider a sparse LEOS constellation, and hence the ground users connect to only one satellite during its flyover period [58], [59].

A. LEOS Transmitter Model

In the considered system model, the LEOS transmits data to two ground users, using NOMA as shown in Fig. 1. The two users are denoted as NU for the NU and FU for the FU. To provide reliable data transmission, Type-I ARQ is used where erroneous packets for both users can be retransmitted. The LEOS sends M packets to each user sequentially through a wireless link using T TSs, $\mathrm{TS}_1, \mathrm{TS}_2, \ldots, \mathrm{TS}_T$, and uses the truncated stop-and-wait (SW) protocol with a maximum of L transmissions for each user packet [28], and hence $M \leq T \leq LM$. Therefore, the LEOS should buffer the last packet for each user until the two packets are received correctly or dropped. In conventional ARQ systems, once a packet is dropped at the receiver, no further effort is made to recover such packets. Therefore, ARQ is useful only before a packet is dropped. To enable packet error detection, we assume that cyclic redundancy check (CRC) bits are appended to each transmitted packet. A packet is considered dropped if it fails CRC after L transmissions. The CRC bits for all packets are assumed to be accessible by both users.

Given that the LEOS and the ground users are equipped with a single antenna each, the transmitted two-user NOMA packet during current transmission is expressed as

$$\mathbf{s}_{i,j}^{(\ell_N,\ell_F)} = \sqrt{p_{N,i}^{(\ell_N)}}\ \mathbf{a}_i^{(\ell_N)} + \sqrt{p_{F,j}^{(\ell_F)}}\ \mathbf{b}_j^{(\ell_F)} \tag{1}$$

where ℓ_N and ℓ_F, respectively, are the transmission counters of both packets, i.e., packets for the NU and the FU, $p_{N,i}^{(\ell_N)}$ and $p_{F,j}^{(\ell_F)}$ are the transmission powers for the ith and jth packets for the NU and FU, respectively, during their ℓ_Nth and ℓ_Fth transmission session. The total power of all users is normalized so that $p_{N,i}^{(\ell_N)} + p_{F,j}^{(\ell_F)} = 1$ and the power for each user should satisfy the constraints described in [18]. The sequences $\{\mathbf{a}_i^{(\ell_N)}, \mathbf{b}_j^{(\ell_F)}\}$ are the ith and jth transmitted data packets for the NU and FU, and each packet consists of K data symbols. The total number of bits transmitted per packet is $B_u = K \log_2(\mathcal{M}_u)$, $u \in \{N, F\}$, where $\mathcal{M}_u$ is the modulation order. Although the proposed system can be applied using dynamic power allocation, a fixed power allocation is adopted in this work for design tractability. Therefore, the powers of NU and FU can be written as $p_N = p_{N,i}^{(\ell_N)}$ and $p_F = p_{F,j}^{(\ell_F)}$.

B. Channel Model

The amplitude of a LEOS channel is affected by several factors, such as beam gain, rain, and fog attenuation, atmospheric

absorption, and small-scale fading due to multipath reflection, and large-scale fading. The amplitude variation due to these factors is generally slow, even at relatively high-Doppler shifts, and therefore the channel envelope can be considered constant over the intervals of interest [60]. Unlike the amplitude, the channel phase is more sensitive to channel variations caused by satellite mobility. Consequently, tight phase tracking is needed to avoid performance degradation due to imperfect phase estimation and compensation [61], [62], [63]. In this work, the channel between the LEOS and NU is indicated by h, whereas the channel for FU is indicated by g. Because the distance between the two users is very large, the channels' coefficients h and g are considered to be independent and identically distributed (i.i.d.). Therefore, the channels for the near and far users are given, respectively, by: $h = |h_R|e^{j\theta_R} + |h_D|e^{j\theta_D}$ and $g = |g_R|e^{j\phi_R} + |g_D|e^{j\phi_D}$ [64]. The combined effect of the scattering components between each ground user and the LEOS is characterized by a Rayleigh distributed amplitude $|h_R| \sim \mathcal{R}(d_N^{-\eta})$ and $|g_R| \sim \mathcal{R}(d_F^{-\eta})$, where d_N and d_F denote the distances between the satellite and the NU and FU, respectively, and η is the pathloss exponent. The phase is considered random with uniform distribution $\{\theta_R, \phi_R\} \sim \mathcal{U}[-\pi, \pi]$. The second part of the channels, that is $|h_D|$ and $|g_D|$ represents the line of sight (LOS) component of the channel, which typically has a deterministic amplitude and phase. To capture the various impairments of the channel and imperfections of the system, the LOS component is suppressed, which corresponds to a severe fading scenario. In LEOS systems, the distances between the satellite and the ground users vary based on the position of the satellite in orbit. Therefore, the designation of near- and FUs is considered for a given realization over a short time period. Over long time periods, the power allocation factors should be based on the position of the satellite in orbit to take into account the distances to the ground users.

Based on the given transmitted packets and channel model, the received sequences at the NU and FU can be written, respectively, as

$$\mathbf{r}_{N,i,j}^{(\ell_N,\ell_F)} = h_i^{(\ell_N)} \mathbf{s}_{i,j}^{(\ell_N,\ell_F)} + \mathbf{n}_{i,j}^{(\ell_N)} \tag{2}$$

$$\mathbf{r}_{F,i,j}^{(\ell_N,\ell_F)} = g_j^{(\ell_F)} \mathbf{s}_{i,j}^{(\ell_N,\ell_F)} + \mathbf{w}_{i,j}^{(\ell_F)} \tag{3}$$

where $\mathbf{n}_{i,j}^{(\ell_N)}$ and $\mathbf{w}_{i,j}^{(\ell_F)}$ are the additive white Gaussian noise (AWGN) vectors where each element in these vectors is represented as $\mathcal{CN}(0, \sigma^2)$. Furthermore, all AWGN samples are mutually independent for all i, j, ℓ_N, and ℓ_F.

III. Overview of NOMA Receiver Design

This section presents an overview of various NOMA receiver designs and the mathematical formulation that will be used throughout this article.

A. Near-User Receiver Without Combining

Because the NU packet is multiplexed with low power, the NU should detect the FU packet first and then use SIC to cancel the interference caused by the FU, and then it can detect its own packet. Therefore, the detection of the FU packet is denoted as

$$\hat{\mathbf{b}}_j = \mathcal{D}_F\left\{\mathbf{r}_{N,i,j}^{(\ell_N,\ell_F)}\right\} \tag{4}$$

where $\mathcal{D}_F\{\cdot\}$ represents the single-user maximum likelihood detection (MLD) operation because the NU signal at this stage is considered as unknown additive noise. The NU packet is detected by applying SIC to eliminate the impact of $\hat{\mathbf{b}}_j$. Therefore, the received signal after SIC can be expressed as

$$\check{\mathbf{r}}_{N,i,j}^{(\ell_N,\ell_F)} = \mathbf{r}_{N,i,j}^{(\ell_N,\ell_F)} - \hat{h}_i^{(\ell_N)} \sqrt{p_F}\, \hat{\mathbf{b}}_j \tag{5}$$

where $\hat{h}$ is the estimated channel coefficient. Then, a single-user MLD, denoted as $\mathcal{D}_N\{\cdot\}$, is used

$$\hat{\mathbf{a}}_i = \mathcal{D}_N\left\{\check{\mathbf{r}}_{N,i,j}^{(\ell_N,\ell_F)}\right\}. \tag{6}$$

Generally speaking, the MLD for the two users can be different, and thus they were given different notations. The MLD of the FU, SIC, and MLD of the NU at the NU receiver are denoted as

$$\left\{\hat{\mathbf{b}}_j, \hat{\mathbf{a}}_i\right\} = \tilde{\mathcal{D}}_N\left\{\mathbf{r}_{N,i,j}^{(\ell_N,\ell_F)}\right\}. \tag{7}$$

It is worth noting that the detection process of the FU symbols affects the detection process of the NU symbols. That is, if $\hat{\mathbf{b}}_j \neq \mathbf{b}_j$, then the SIC process will fail and most likely we obtain $\hat{\mathbf{a}}_i \neq \mathbf{a}_i$. Therefore, given that the NU has access to the CRC bits of the FU, detection of $\mathbf{a}_i$ using $\mathcal{D}_N$ is carried out when $\mathbf{b}_j$ successfully passes the CRC process. Otherwise, a NACK is sent to the LEOS to indicate that $\mathbf{a}_i$ was received incorrectly. If the number of transmissions for $\mathbf{a}_i$ is equal to L, i.e., if $\ell_N = L$, and $\hat{\mathbf{a}}_i$ fails the CRC, then $\mathbf{a}_i$ is declared dropped.

B. Near-User Receiver With Combining

In the event that $\mathbf{a}_i$ is not received correctly, it will be retransmitted up to L times. With sequence combining, the receiver buffers the retransmitted sequences, however, because the buffered sequences consist of packet for two different users, we may obtain the following two possible scenarios.

1) Both receivers send a NACK for packets i and j. Consequently, all received sequences will correspond to the same transmitted NOMA packet $\mathbf{s}_{i,j}^{(\ell_N,\ell_F)}$. Therefore, the NU should buffer

$$\mathbf{r}_{N,i,j}^{(1,1)}, \mathbf{r}_{N,i,j}^{(2,2)}, \ldots, \mathbf{r}_{N,i,j}^{(l,l)}, \quad 1 < l \leq L. \tag{8}$$

In this case, the receiver combines all sequences using CC [28] to produce the sequence $\mathbf{y}_{N,i,j}$

$$\mathbf{y}_{N,i,j} = \frac{\sum_{k=1}^{l} \hat{h}_i^{(k)} \mathbf{r}_{N,i,j}^{(k,k)}}{\sum_{k=1}^{l} \left|\hat{h}_i^{(k)}\right|^2} \triangleq \mathcal{C}\left\{\mathbf{r}_{N,i,j}^{(1,1)}, \ldots, \mathbf{r}_{N,i,j}^{(l,l)}\right\} \tag{9}$$

where $\hat{\bar{h}}$ is the complex conjugate of $\hat{h}$. Then the receiver computes

$$\left\{\hat{\mathbf{b}}_j, \hat{\mathbf{a}}_i\right\} = \tilde{\mathcal{D}}_N\left\{\mathbf{y}_{N,i,j}\right\}. \tag{10}$$

If $l = L$ and $\hat{\mathbf{a}}_i \neq \mathbf{a}_i$, then packet $\mathbf{a}_i$ is dropped by both the LEOS and corresponding receiver.

2) The NU sends a NACK while the FU sends an ACK. Consequently, the received FU sequences will have different values of j. For example, given that the NU sends l NACKs while the FU sends l ACKs, thus the buffered sequences would be

$$\mathbf{r}_{N,i,j}^{(1,1)}, \mathbf{r}_{N,i,j+1}^{(2,1)}, \ldots, \mathbf{r}_{N,i,j+l}^{(l,1)}, \quad 1 < l \leq L. \tag{11}$$

In this case, sequence combining is not straightforward. The conventional system solution is to link both users such that the LEOS sends two new packets, $\mathbf{a}_{i+1}$ and $\mathbf{b}_{j+1}$, only when both users send ACKs for $\mathbf{a}_i$ and $\mathbf{b}_j$ or when the maximum number of transmissions is reached, and thus $i = j$ for all transmissions [65]. Although such a configuration can simplify the system design, it also deteriorates the system throughput because correctly received packets can be retransmitted several times.

C. Far-User Receiver Without and With Combining

Without sequence combining, the FU receiver is similar to the detection in the first stage of the NU. Therefore, a single user MLD is applied to the received NOMA sequence to detect $\mathbf{b}_j$, that is, $\hat{\mathbf{b}}_j = \mathcal{D}_F\{\mathbf{r}_{F,i,j}^{(\ell_N,\ell_F)}\}$.

With sequence combining and using the system model in [65], the combining process is similar to the one at the NU. Therefore, the receiver buffers the corresponding sequences and then combines them using CC [28] to produce the sequence $\mathbf{y}_{F,i,j} = \mathcal{C}\{\mathbf{r}_{F,i,j}^{(1,1)}, \ldots, \mathbf{r}_{F,i,j}^{(l,l)}\}$, and then computes

$$\hat{\mathbf{b}}_j = \mathcal{D}_F\{\mathbf{y}_{F,i,j}\}. \tag{12}$$

D. C-NOMA

In a two-user C-NOMA system, the LEOS transmits the NOMA sequence to both users. The NU implements the protocols described in Section IV-A1 to extract the NU and FU packets from the received NOMA sequence, then the NU forwards the decoded FU packet to the FU. It is assumed that the packet is transmitted through the core TN. Therefore, the FU can have two versions of its own packet, one NOMA sequence received from the LEOS and the other is received from the NU. The FU employs CC to combine both signals before decoding. Consequently, on the ℓth retransmission, the FU combines 2ℓ copies of the same packet, and thus increasing the received SNR and the probability of successful decoding.

IV. Proposed Packet Repair and Recovery

The proposed scheme is composed of three main components, which are A) NOMA combining with asynchronous transmission, B) L-RSIC, and C) C-RSIC.

A. NOMA Combining With Asynchronous Transmission (Online)

As can be seen from the discussion in Section III-B, the sequence that merges in NU is not efficient due to the need to synchronize the retransmissions of the packet sequence numbers of both users, which can cause severe degradation of throughput. Therefore, this work considers the case where sequence combining can be applied without synchronizing the sequence number of the two users, i.e., each user may transmit a new packet regardless of the result of the other user's detection process.

1) NU Receiver: In the case that the received sequences follow the example in (11), then the receiver should first identify the indices of the FU packets to verify if the FU has transmitted the same packet multiple times or not, and thus decide whether direct sequence combining is feasible or not. Toward this goal, we consider that both users share their ACK/NACK through the TN. It is worth noting that the NU can determine whether multiple transmissions have the same or different versions of $\mathbf{b}$ by comparing $\hat{\mathbf{b}}$ with subsequent transmissions, and comparing the difference with a particular threshold.

To simplify the discussion, we consider the initial transmission session where $i = j = \ell_N = \ell_F = 1$. Therefore, the NU receiver design is as follows.

1) Given that $\mathbf{r}_{N,1,1}^{(1,1)}$ is received in the first TS, the receiver first computes $\hat{\mathbf{b}}_1$ using (4), and verifies the CRC bits. If $\hat{\mathbf{b}}_1$ passes the CRC verification, i.e., $\hat{\mathbf{b}}_1 = \mathbf{b}_1$, the receiver proceeds to compute $\check{\mathbf{r}}_{N,1,1}^{(1,1)}$ using (5) and $\hat{\mathbf{a}}_1$ is detected by computing $\mathcal{D}_N L\left\{\check{\mathbf{r}}_{N,1,1}^{(1,1)}\right\}$. If $\hat{\mathbf{a}}_1$ passes the CRC verification process, an ACK is sent to the LEOS and the detection process for $\mathbf{a}_1$ is terminated. However, if $\hat{\mathbf{b}}_1$ passes the CRC verification but $\hat{\mathbf{a}}_1$ does not, the receiver buffers $\mathbf{b}_1$ and $\check{\mathbf{r}}_{N,1,1}^{(1,1)}$.
2) Given that the NU has sent a NACK, the received sequence in the next TS can be either $\mathbf{r}_{N,1,1}^{(2,2)}$ or $\mathbf{r}_{N,1,2}^{(2,1)}$, which depends on the detection outcome of $\mathbf{b}_1$ at the FU. The case of $\mathbf{r}_{N,1,1}^{(2,2)}$ implies that the combining and detection operations can be performed directly as described in (9) and (10). However, in the case of $\mathbf{r}_{N,1,2}^{(2,1)}$, the receiver cannot combine directly. Therefore, it computes $\hat{\mathbf{b}}_2 = \mathcal{D}_F\{\mathbf{r}_{N,1,2}^{(2,1)}\}$ and verifies the CRC bits. If $\hat{\mathbf{b}}_2$ passes the CRC verification, the receiver computes $\check{\mathbf{r}}_{N,1,2}^{(2,1)}$, $\mathbf{y}_N = \mathcal{C}\left\{\check{\mathbf{r}}_{N,1,1}^{(1,1)}, \check{\mathbf{r}}_{N,1,2}^{(2,1)}\right\}$, and $\hat{\mathbf{a}}_1 = \mathcal{D}_N\{\mathbf{y}_N\}$. If $\hat{\mathbf{b}}_2$ fails the CRC, then the combining is infeasible and a NACK is sent to require the retransmission of $\mathbf{a}_1$.
3) The same approach can be applied to all subsequent transmissions. By noting that the FU packets have much higher power than the NU packets, they most likely will be detected correctly at the NU, which implies that combining is feasible even if different packets are transmitted in each TS.

2) FU Receiver: The FU receiver is generally unchanged with and without user synchronization. Therefore, we consider in this work that the FU always combines all transmissions that correspond to a particular $\mathbf{b}$.

B. Local RSIC (Offline)

If the packet detection process at the near and/or far users fails for L consecutive times after applying the NOMA combining, then the packet is dropped and the receiver should apply the L-RSIC to try repairing and recovering the dropped packet. The proposed L-RSIC is designed to avoid discarding

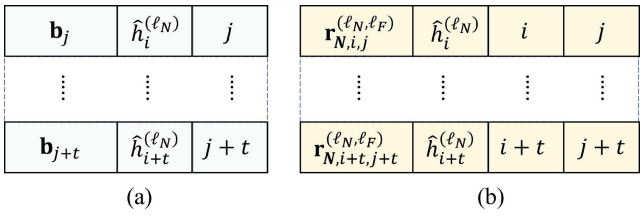

Fig. 2. NU buffers (a) $\mathbb{A}_N$ to store decoded FU packets and other related information at the NU. (b) $\mathbb{B}_N$ to store the whole received signals and the related information if the NU packet does not pass CRC check.

Algorithm 1: Near (Far) User Tracking Far (Near) User's Indices

$\mathbb{U} \in$ {Near-user, Far-user}
$x \in \mathbb{U},\ y \in \mathbb{U} \setminus x$
Input: $L, A_y, \ell_y, \bar{I}_y$
Output: $I_y \in \{i, j\}$ ▷ Index of y
if $\{A_y = 0\}$ ***and*** $\{\ell_y < L\}$ **then**
  $I_y \leftarrow \bar{I}_y$
  $\ell_y \leftarrow \ell_y + 1$
else
  $I_y \leftarrow \bar{I}_y + 1$
  $\ell_y \leftarrow 1$

information that may be used for further processing by the user itself or by the other user. Therefore, each user will have four buffers, where each buffer is used to store certain information. The buffers are denoted as $\mathbb{A}$, $\mathbb{B}$, $\mathbb{C}$, and $\mathbb{D}$, and a subscript, N or F, is added to denote the near and far users, respectively. As an example, Fig. 2 shows buffers for the NU where $\mathbb{A}_N$ stores $\mathbf{b}_j$ $\forall j$, which are the FU packets that were detected correctly at the NU receiver, as well as the corresponding channel coefficients and packets' indices. Buffer $\mathbb{B}_N$ stores the received NOMA sequence, the corresponding channel coefficients, and indices of the NU and FU packets. Buffer $\mathbb{C}_N$ only stores $\mathbf{r}_{N,i,j}^{(L,\ell_F)}$ for the dropped packets in addition to the estimated channel coefficient $\hat{h}_i^{(L)}$. The buffer $\mathbb{D}_N$ is used to store successfully detected packets of NU and their index i, which is known at the NU. Furthermore, the receiver determines the FU packet index j through the ACK/NACK received from the FU as described in Algorithm 1. Because the ACKs/NACKs have a low-data rate, it is reasonable to consider that they are shared through an error-free TN. Although the NU receiver detects the FU packets, it only returns the ACK/NACK for its own packets. The symbols used in Algorithm 1 are defined in Table I.

In summary, if the detection of a certain packet that belongs to a certain user fails, the received NOMA sequence, its corresponding $\hat{h}$ and index, i or j, are saved in buffer $\mathbb{B}$, and a NACK is returned. If $\ell = L$, the packet is considered dropped, and the current received NOMA sequence is stored in the dropped packets buffer $\mathbb{C}$. If the packet is detected successfully, an ACK is returned, and the decoded packet is stored in $\mathbb{D}$. In all scenarios, the ACK/NACK sent by a given user is received by both the LEOS and other user.

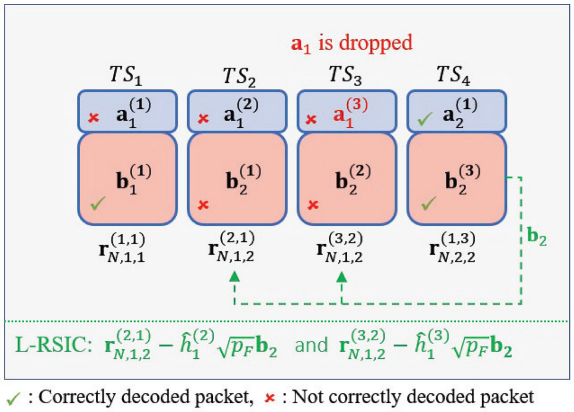

Fig. 3. Example of offline L-RSIC at the NU receiver, $L = 3$.

TABLE I
LIST OF SYMBOLS USED IN ALGORITHM 1

Notation	Explanation
x, y	Represent the NU and FU users
L	Max. no. of allowed transmission per packet
A_y	ACK from y
ℓ_y	Retransmission counter of y
$\bar{I}_y$	Index of y's packet in the last transmission
I_y	Index of y's packet estimated by x. $I_y = i$ if the algorithm is run by FU receiver. Otherwise, $I_y = j$ if the algorithm is run by NU receiver

To simply the presentation, a specific reception scenario is presented in Fig. 3. The figure shows the L-RSIC at the NU receiver. In this example, it is assumed that transmission is carried out over 4 time intervals and $L = 3$ for both users. It is shown that packet $\mathbf{a}_1$ is dropped after 3rd time-slot, i.e., when $\ell_N > 3$. During the first transmission of $\mathbf{a}_1$, $\ell_N = 1$, the FU packet is $\mathbf{b}_1$, whereas during the second and third transmissions of $\mathbf{a}_1$, the FU has $\mathbf{b}_2$ in both intervals. This is because the FU has decoded $\mathbf{b}_1^{(1)}$ correctly while $\mathbf{b}_2^{(1)}$ and $\mathbf{b}_2^{(2)}$ failed. Furthermore, the figure shows that the NU successfully decodes $\mathbf{b}_1^{(1)}$ during TS_1. Therefore, a correctly decoded version of $\mathbf{b}_1^{(1)}$ is stored in the local buffer $\mathbb{A}_N$. In TS_4, the NU receives $\mathbf{r}_{N,2,2}^{(1,3)}$ NOMA sequence, which is composed of $\mathbf{a}_2^{(1)}$ and $\mathbf{b}_2^{(3)}$, and both packets are correctly decoded.

Because $\mathbf{a}_1$ is dropped and the satellite flyover is completed, the offline L-RSIC is launched by the NU receiver to recover the dropped $\mathbf{a}_1$. It should be noted that $\mathbf{b}_2$ shares the second and third TSs with $\mathbf{a}_1$, and creates significant interference for $\mathbf{a}_1$ due to its incorrect detection in both slots, leading to a SIC failure. By noting that $\mathbf{b}_2$ was detected correctly in TS_4, then RSIC can be applied by subtracting the effect of $\mathbf{b}_2$ from $\mathbf{r}_{N,1,2}^{(2,1)}$ and $\mathbf{r}_{N,1,2}^{(3,2)}$ to get $\check{\mathbf{r}}_{N,1,2}^{(2,1)}$ and $\check{\mathbf{r}}_{N,1,2}^{(3,2)}$. Similarly, the correctly decoded $\mathbf{b}_1^{(1)}$ is used to remove the interference from $\mathbf{r}_{N,1,1}^{(1,1)}$ to get $\check{\mathbf{r}}_{N,1,1}^{(1,1)}$. The three resultant sequences are then combined as $\mathcal{C}\left\{\check{\mathbf{r}}_{N,1,2}^{(2,1)}, \check{\mathbf{r}}_{N,1,2}^{(3,2)}, \check{\mathbf{r}}_{N,1,1}^{(1,1)}\right\}$, and a decoding attempt is applied to the combined realization.

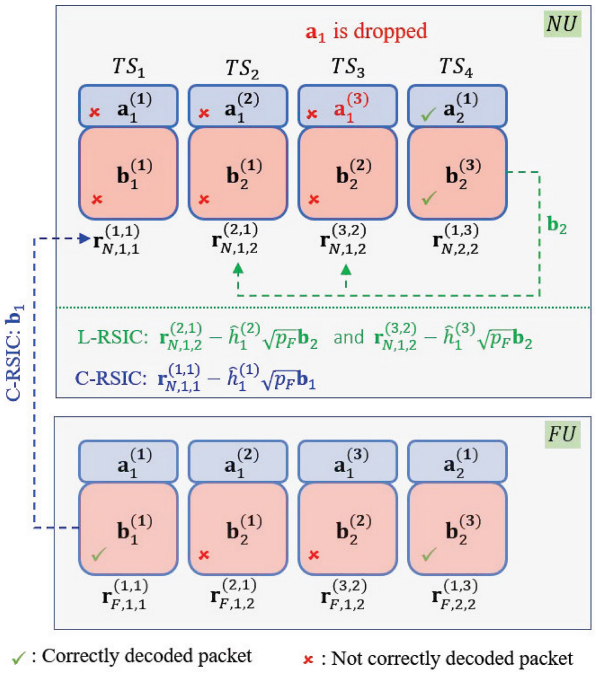

Fig. 4. Example of offline C-RSIC and L-RSIC at the NU receiver, $L = 3$.

Algorithm 2: Offline Packet Recovery at NU

Input: $n_D \leftarrow$ No. of dropped packets in NOMA phase
foreach *packet in* $\mathbb{C}_N$ **do**
  $\mathcal{X} \leftarrow \emptyset$
  $\mathbf{M} \leftarrow$ extract L versions of last dropped packet from $\mathbb{B}_N$
  for $k \in \{1, 2, \ldots, L\}$ **do**
    $\mathbf{m} \leftarrow k$th row from $\mathbf{M}$
    $[i, j] \leftarrow$ extract NU and FU indices from $\mathbf{m}$
    if $\mathbf{b}_j \in \mathbb{A}_N$ **then**
      fetch $\mathbf{b}_j$ from $\mathbb{A}_n$ ▷ L-RSIC
    else if $\hat{\mathbf{b}}_j = \mathbf{b}_j$ *at FU* **then**
      fetch $\mathbf{b}_j$ from FU ▷ C-RSIC
    else
      continue
    compute $\check{\mathbf{r}}_{N,i,j}^{(k,\ell_F)}$ using $\mathbf{b}_j$ and (5)
    $\mathcal{X} \leftarrow \mathcal{X} \cup \{\check{\mathbf{r}}_{N,i,j}^{(k,\ell_F)}\}$
    $\mathbf{d}_1 \leftarrow \mathcal{C}\{\mathcal{X}\}$, $\hat{\mathbf{a}}_i \leftarrow \mathcal{D}_N\{\mathbf{d}_1\}$
    if $\hat{\mathbf{a}}_i = \mathbf{a}_i$ **then**
      remove the realization of packet with index i from $\mathbb{C}_N$
      add $\mathbf{a}_i$ to $\mathbb{D}_N$
      $n_D \leftarrow n_D - 1$
      break

C. Cooperative RSIC (Offline)

1) Near User: The example used to describe the C-RSIC is shown in Fig. 4. For this scenario, the first three detection processes for $\mathbf{a}_1$ have failed, and thus the packet is dropped. The associated FU packets, $\mathbf{b}_1$ in TS_1 and $\mathbf{b}_2$ in TS_2 and TS_3, also were not detected correctly at the NU. However, $\mathbf{b}_2$ is correctly detected in TS_4. Based on the proposed protocol, the first action step in this case is to apply the L-RSIC using the correctly detected version of $\mathbf{b}_2$. Assuming that the L-RSIC has failed, the C-RSIC can be applied because $\mathbf{b}_1$ was detected correctly by the FU. Therefore, the NU receiver requests the FU to share $\mathbf{b}_1$, which is eventually used to eliminate the interference from $\mathbf{r}_{N,1,1}^{(1,1)}$ to obtain $\check{\mathbf{r}}_{N,1,1}^{(1,1)}$. Consequently, the L-RSIC and C-RSIC produce the interference-free sequences $\check{\mathbf{r}}_{N,1,2}^{(2,1)}$, $\check{\mathbf{r}}_{N,1,2}^{(3,2)}$, and $\check{\mathbf{r}}_{N,1,1}^{(1,1)}$, which correspond to $\mathbf{a}_1$. Therefore, $\hat{\mathbf{a}}_1$ can be obtained by applying CC to the three sequences and then applying MLD.

The offline packet recovery process at the NU receiver is described in Algorithm 2. The algorithm iterates over the dropped packets in $\mathbb{C}_N$ buffer in an attempt to recover them. The NU retrieves L versions of the most recently dropped packet from buffer $\mathbb{B}_N$. Starting with the most recent version, NU packets are extracted from each realization. The indices i and j of the NU and FU are extracted from the dropped packet. Subsequently, the jth FU packet, if present in the buffer $\mathbb{A}_N$, is used to compute the SIC and detect the ith NU packet. If the jth FU packet is available only in $\mathbb{A}_F$, the FU will send it to the NU. If the jth FU packet is not present in either $\mathbb{A}_N$ or $\mathbb{A}_F$, the corresponding NU packet will not be applied to the detector. The currently stored versions of NU sequences after SIC are combined using CC, and an attempt is made to detect the combined packets. If the detected NU packet passes the CRC process, it is stored in the decoded buffer $\mathbb{D}_N$, along with the NU index i. Furthermore, the correctly detected ith packet is removed from the drop buffer $\mathbb{C}_N$.

2) Far User: The offline recovery process of the FU receiver is described in Algorithm 3. The algorithm traverses the $\mathbb{C}_F$ buffer, which contains the dropped packets. The L versions of the most recent dropped packet are retrieved from buffer $\mathbb{B}_F$. Subsequently, the indices of the NU and FU packets are extracted, beginning with the Lth realization. If the NU packet is available in the NU buffer $\mathbb{D}_N$, indicating that the NU correctly detected the ith packet, it is shared with the FU. To obtain the required FU received sequences without interference, the FU receiver applies SIC using the shared NU packet to the corresponding NOMA sequence and then detects its own packet. However, if the ith NU packet is not available in the NU buffer $\mathbb{D}_N$, the FU asks for the $(i+1)$th NU packet if it is different from the ith packet and it is part of the NOMA sequence that corresponds to $\mathbf{b}_j$. If none of the NU packets can be shared, the FU packet is permanently dropped. Otherwise, the FU combines all realizations after a full or partial interference cancelation to get $\mathbf{b}_j^{(\ell_F)}$. If $\mathbf{b}_j^{(\ell_F)}$ passes the CRC, the jth dropped packet is removed from the buffer $\mathbb{C}_F$, while the correctly recovered packet $\mathbf{b}_j^{(\ell_F)}$ is added in the decoded buffer $\mathbb{D}_F$. The offline packet recovery process is executed iteratively by both users, allowing them to retrieve additional dropped packets that were not repaired or recovered during the initial phases.

D. Practical Considerations

To investigate the feasibility of integrating the proposed solution into practical LEOS systems, this section evaluates the various practical aspects of the proposed system, namely,

Algorithm 3: Offline Packet Recovery at FU

Input: $f_D \leftarrow$ No. of dropped packets in NOMA phase
1 $f_{1\times L} \leftarrow [0, 0, \ldots, 0]$
2 **foreach** *packet in* $\mathbb{C}_F$ **do**
3 $\quad \mathcal{X} \leftarrow \emptyset$
4 $\quad \mathbf{M} \leftarrow$ extract L versions of last dropped packet from $\mathbb{B}_F$
5 $\quad$ **for** $k \in \{1, 2, \ldots, L\}$ **do**
6 $\quad\quad$ **if** $f(k) = 0$ **then**
7 $\quad\quad\quad \mathbf{m} \leftarrow k$th row from $\mathbf{M}$
8 $\quad\quad\quad [i, j] \leftarrow$ extract NU and FU indices from $\mathbf{m}$
9 $\quad\quad\quad$ **if** $\hat{\mathbf{a}}_i = \mathbf{a}_i$ *at NU* **then**
10 $\quad\quad\quad\quad$ fetch $\mathbf{a}_i$ from NU ▷ C-RSIC
11 $\quad\quad\quad\quad$ apply SIC to compute $\check{\mathbf{r}}_{F,i,j}^{(\ell_N,k)}$ using $\mathbf{a}_i$
12 $\quad\quad\quad\quad \mathcal{X} \leftarrow \mathcal{X} \cup \{\check{\mathbf{r}}_{N,i,j}^{(\ell_N,k)}\}$
13 $\quad\quad\quad\quad f(k) \leftarrow 1$
14 $\quad\quad\quad$ **else**
15 $\quad\quad\quad\quad c \leftarrow$ no. of identical $\{\mathbf{a}_i, \mathbf{b}_j\}$ packets in $\mathbf{M}$
16 $\quad\quad\quad\quad$ **for** $q \in \{k, \ldots, k + c - 1\}$ **do**
17 $\quad\quad\quad\quad\quad \mathbf{r}_{F,i,j}^{(\ell_N,q)} \leftarrow q$th row from $\mathbf{M}$
18 $\quad\quad\quad\quad\quad \mathcal{X} \leftarrow \mathcal{X} \cup \{\mathbf{r}_{F,i,j}^{(\ell_N,q)}\}$
19 $\quad\quad\quad\quad\quad f(q) \leftarrow 1$
20 $\quad\quad$ $\mathbf{d}_1 \leftarrow \mathcal{C}\{\mathcal{X}\}$, $\hat{\mathbf{b}}_j \leftarrow \mathcal{D}_F\{\mathbf{d}_1\}$
21 $\quad\quad$ **if** $\hat{\mathbf{b}}_j = \mathbf{b}_j$ **then**
22 $\quad\quad\quad$ remove the realization of packet with index j from $\mathbb{C}_F$
23 $\quad\quad\quad$ add $\mathbf{b}_j$ to $\mathbb{D}_F$
24 $\quad\quad\quad f_D \leftarrow f_D - 1$
25 $\quad\quad\quad$ **break**

the system configuration, computational complexity, storage requirements and delay, energy and computational power.

1) System Configuration: The proposed system can be seamlessly integrated with existing LEOS systems because it mostly affects the receivers of the ground users. Specifically, ARQ is typically part of all flow control protocols, and the proposed system does not require any modification to the conventional ARQ. At the LEOS transmitter, NOMA should be integrated to combine the data of both users, and transmission power assignment can be performed based on the distance from each ground user. Therefore, the total modifications at the LEOS are generally insignificant. For the TN, the two ground users should be connected via a wired low-latency connection. Therefore, the main elements of the proposed system are implemented at the ground users.

2) Computational Complexity: In this section, we examine the computational complexity, in the worst case, of the proposed offline RSIC algorithm for both NU and FU scenarios. The complexity is expressed using the big $\mathcal{O}$ notation. The RSIC system includes fixed-cost operations, such as sequence extraction, $\mathcal{C}\{\cdot\}$ operation, SIC, and MLD.

For the $\mathcal{C}\{\cdot\}$ operation in (9), the numerator is computed by adding a maximum of L sequences of size K where each sequence is multiplied by a complex number. The denominator is the sum of a maximum of L scalars, each calculated as the squared magnitude of a complex number. Therefore, the overall complexity of the $\mathcal{C}\{\cdot\}$ operation is $\mathcal{O}(LK)$. Without loss of generality, and for this analysis, we assume $\mathcal{M}_N = \mathcal{M}_F = \mathcal{M}$. For MLD (4), the complexity is $\mathcal{O}(\mathcal{M})$. The complexity of the SIC operation (5) is $\mathcal{O}(K)$.

a) NU complexity: The worst case complexity corresponds to the case where all NU packets are dropped, and thus, buffer $\mathbb{C}_N$ has a total of M entries. Therefore, the *foreach* loop spanning Line 2 to Line 20 of Algorithm 2 will iterate M times. The *for* loop at Line 4 will be executed L times. This loop includes operations, such as extracting the indices of the sequences, $\mathcal{C}\{\cdot\}$ operation, SIC, and MLD. As a result, the overall complexity of the proposed RSIC algorithm for the NU is $\mathcal{O}(LM \times (LK + \mathcal{M} + K)) \approx \mathcal{O}(MK)$, where $L \ll M$ and L usually has small values. Therefore, the complexity is linear in nature.

b) FU complexity: Following a similar analysis, it is found that the overall computational complexity of the RSIC at the FU is equivalent to that of NU.

3) Storage Requirements and Delay: Unlike traditional NOMA, the proposed system requires the inclusion of additional buffers $\mathbb{A}$, $\mathbb{B}$, $\mathbb{C}$, and $\mathbb{D}$. The buffer $\mathbb{A}$ stores $M \times B_u$ bits, while the size of $\mathbb{B}$ depends on the desired quantization errors, which is assumed to be 8 bits for each received sample and another 8 bits for the corresponding channel coefficient. Therefore, the size of $\mathbb{B}$ is equal to $16K \times L \times M$. Similarly, the size of $\mathbb{C}$ is $16K \times M$. The size of buffer $\mathbb{D}$ is similar to that of $\mathbb{A}$. For example, assuming that the satellite will transmit two images, each of which has a size of 10 MB modulated using binary phase shift keying (BPSK) with $L = 3$, thus the storage requirements are $\{10, 480, 160, 10\}$ MB for buffers $\mathbb{A}$, $\mathbb{B}$, $\mathbb{C}$, and $\mathbb{D}$, respectively. Consequently, the total storage required for the two images is 660 MB for each ground user. Therefore, the total storage depends on the number of images transmitted per flyover. For LEOS, the flyover time is typically in the order of a few minutes, which implies that the number of images transmitted per flyover is very small, and hence the storage requirements are within the capacity of any ground user. The processing time for each image depends on the SNR, i.e., the number of packets dropped. Tables II and III show the simulation time, sec. per MB, of the offline packet repair and recovery process. As can be seen from the results, the processing times may range from a few minutes to a fraction of a second. Therefore, all images can be processed, and buffers can be cleared prior to the next flyover. The time complexity is evaluated using MATLAB on a system with an Intel Core i7-9750H CPU @ 2.60 GHz with 16 GB RAM. The total number of packets transmitted to each user during the NOMA phase is $M = 10^5$, and each packet contains $K = 128$ symbols.

TABLE II
L-RSIC AND C-RSIC SIMULATION TIME (S) PER MB FOR $\gamma_{\text{TN}} = 0$ DB

L	p_N	SNR (dB)					
		8	12	16	20	24	28
2	0.1	128.70	39.48	9.69	2.03	0.74	0.42
	0.2	90.97	41.47	10.49	3.10	0.83	0.45
3	0.1	90.90	15.91	1.90	0.48	0.38	0.16
	0.2	80.30	20.53	3.99	0.75	0.43	0.36

TABLE III
L-RSIC AND C-RSIC SIMULATION TIME (S) PER MB FOR $\gamma_{\text{TN}} = 50$ DB

L	p_N	SNR (dB)					
		8	12	16	20	24	28
2	0.1	280.41	98.66	24.31	4.99	1.23	0.48
	0.2	181.28	83.62	21.05	4.99	1.46	0.58
3	0.1	222.40	42.15	5.01	0.65	0.40	0.18
	0.2	159.74	34.04	6.04	0.98	0.50	0.43

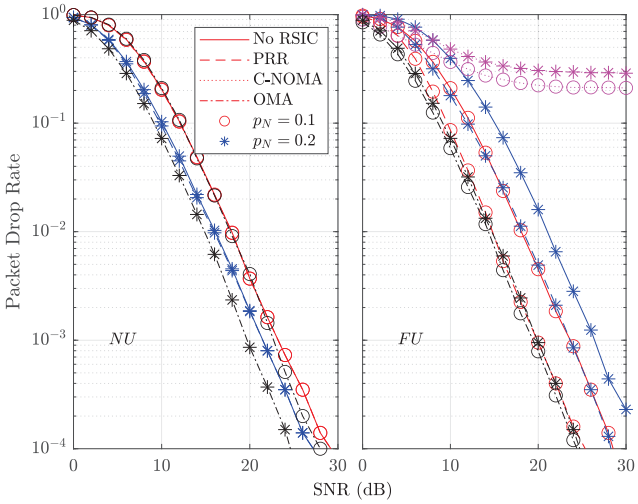

Fig. 5. PDR for $\gamma_{\text{TN}} = 0$ dB with $L = 2$.

4) Energy and Computational Power: The total energy and computational power required are generally comparable to those of conventional systems to perform basic computations, such as detection and combining. And hence it should not be considered a burden for the ground users processing machines.

V. NUMERICAL RESULTS AND DISCUSSIONS

This section presents the performance evaluation of the proposed PRR with and without offline RSIC, and compares it with the C-NOMA. The performance is evaluated in terms of PDR, number of packets dropped, number of packets recovered using the offline RSIC, and throughput achieved by both users. The results are obtained for SNR values ranging from 0 to 30 dB, the maximum number of transmissions permitted per packet $L \in \{2, 3\}$ for both users. The normalized transmission powers $\{p_N, p_F\} \in \{\{0.1, 0.9\}, \{0.2, 0.8\}\}$, and the information bits are modulated using BPSK. The channel between terrestrial users is modeled as a Rayleigh fading channel to capture the various impairments that may exist in the TN, and the SNR between the two users during packet exchange for offline RSIC is considered to be $\gamma_{\text{TN}} \in \{0, 50\}$ dB. The packet length for each user is considered to have $B = 128$ bits. Each Monte Carlo simulation point is obtained using $M = 10^5$ NOMA transmissions. The performance improvement is measured at PDR$= 10^{-3}$. The distances between the LEOS and ground users are selected such that $d_F = 2d_N$ and the path loss exponent $\eta = -2$.

The simulation results for the PDR of NU and FU are shown in Figs. 5–8. For the OMA simulation, results for NU are obtained by transmitting OMA packets using $p_N = \{0.1, 0.2\}$. Similarly, results for FU are achieved by sending OMA packets to FU with $p_F = \{0.8, 0.9\}$. All other simulation parameters in the OMA simulation are to NOMA simulations. Fig. 5 shows the PDR for $\gamma_{\text{TN}} = 0$ dB and $L = 2$. As can be seen from the figure, the NU PDR improves by about 1.8 dB when p_N increases from 0.1 to 0.2. The impact of RSIC on the NU PDR is marginal because the FU packets have high power and will most of the time be detected correctly, leading to successful interference cancelation. Comparing OMA and NOMA shows that OMA outperforms the PRR because the interference in the NOMA case was not successfully canceled in several cases. For the FU, the figure shows a significant improvement in terms of PDR when its transmission power increases from $p_F = 0.8$ to $p_F = 0.9$. Moreover, it can be noted that an additional significant improvement is observed using the proposed PRR. The PRR in this case performs well because its packets are the ones that determine the outcome of the detection process. Therefore, interference cancelation in this case can be very efficient in terms of packet repair and recovery. It is interesting to note that for $p_N = 0.1$, the OMA

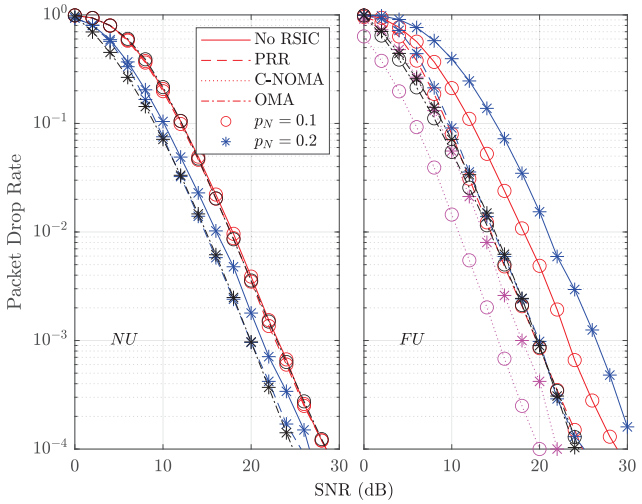

Fig. 6. PDR for $\gamma_{\text{TN}} = 50$ dB with $L = 2$.

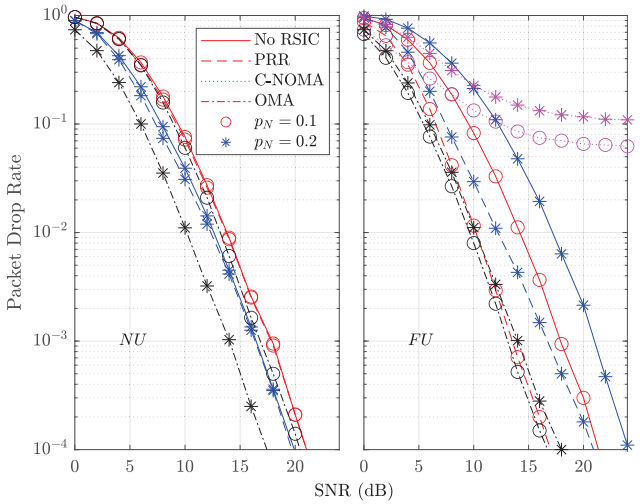

Fig. 7. PDR for $\gamma_{\text{TN}} = 0$ dB with $L = 3$.

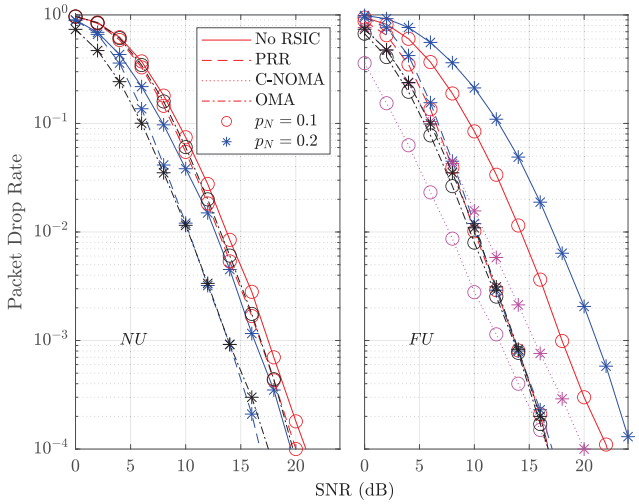

Fig. 8. PDR for $\gamma_{\text{TN}} = 50$ dB with $L = 3$.

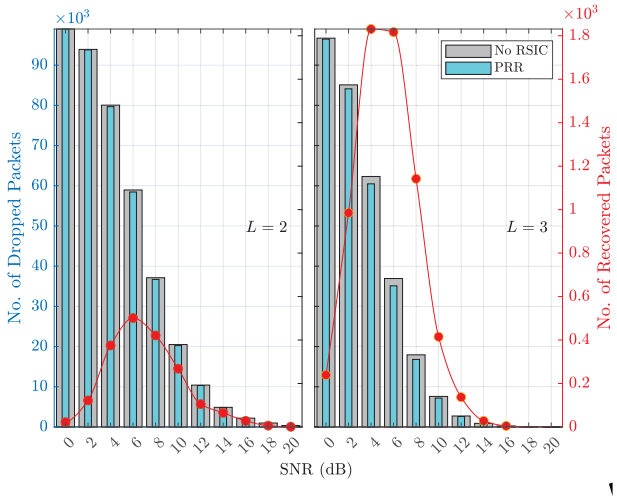

Fig. 9. Number of dropped and recovered packets for $\gamma_{\text{TN}} = 0$ dB at the NU receiver with $p_N = 0.1$.

and NOMA offer comparable performance. The C-NOMA has the worst performance because the FU combines the packets received from the NU over the extremely noisy TN channel where $\gamma_{\text{TN}} = 0$ dB in this case. As a result, the probability of correctly detecting the FU packet decreases drastically. It is worth mentioning that changing p_N from 0.1 to 0.2 improves the OMA performance at the NU by 3 dB while the improvement is 0.5 dB for the FU.

Fig. 6 shows the PDR of both users for $\gamma_{\text{TN}} = 50$ dB. As can be seen from the figure, the NU PDR slightly improves when the SNR between the users increases from 0 to 50 dB. This scenario is similar to Fig. 5 where interference has a limited impact. For the FU, the proposed PRR outperforms the no PRR scenario by approximately 6 dB. This performance is obtained due to the high γ_{TN}, which improves the quality of the packets sent from the NU to the FU. The effectiveness of the PRR can be observed from the equivalent PDR for the cases of $p_N = 0.1$, 0.2, and OMA, because it implies that most of the packets dropped due to interference were recovered. The impact of increasing γ_{TN} is also significant for the C-NOMA case where its performance improves significantly. For such a high γ_{TN}, the FU packets decoded and forwarded by the NU are highly reliable, and therefore, when FU combines them with the packets received from the LEOS, their overall SNR improves considerably.

Fig. 7 shows the PDR for the NU and FU for $L = 3$ and $\gamma_{\text{TN}} = 0$ dB. Compared to $L = 2$ in Fig. 5, a significant improvement is realized for all cases due to the additional transmission allowed. Generally speaking, all schemes benefited by about 6 dB, except for C-NOMA due to the error floor caused by combining the nonreliable packets forwarded by the NU. The relative performance gain with and without PRR is more than the case of $L = 2$, particularly for the FU where the gain is about 4.25 dB for $p_N = 0.2$ and 4.4 dB for $p_N = 0.1$.

Fig. 8 evaluates the case of $L = 3$ and $\gamma_{\text{TN}} = 50$ dB while keeping all other parameters unchanged. Compared to Fig. 7, it can be seen that the NU achieves about 5 dB gain with $p_N = 0.1$ and the FU achieves around 4.4 dB gain with $p_N = 0.2$ and 7.3 dB with $p_N = 0.1$. The C-NOMA outperforms the proposed PRR for the FU at low-SNR range. This is because the channel between the ground users is strong and FU combines 2ℓ packets instead of ℓ packets with the PRR. However, during the PRR phase, the FU gets the NU packets over the same strong channel. This, in turn, improves its performance compared to C-NOMA under good SNR conditions.

Figs. 9–16 show the number of packets dropped with and without offline RSIC, left y axis. The right y-axis is associated with the line graphs and represents the number of recovered packets. The general trends that can be seen in all scenarios are as follows.

1) The number of initial drops at the NU and FU is generally comparable, which is due to the fact the product of the average channel gain and transmission power are close. For example, the ratio of the initially dropped packets for the NU in Fig. 9 and FU in Fig. 11 ranges between 1.1% and 7.3%.
2) For both users, increasing the value of L improves the performance of RSIC where the number of recovered packets increases. This performance is obtained because increasing L also increases the number of correlated dropped packets. Consequently, using the RSIC becomes more impactful. The number of initially dropped packets would definitely decrease as L increases due to the additional diversity gain introduced. For the results in Fig. 9, the ratios of the initially dropped packets with $L = 3$ to that of $L = 2$ for SNR $= 0, 2, \ldots, 16$ are, respectively, given by [97.7, 90.6, 77.8, 62.6, 48.3, 37.0, 26.2, 18.3, 11.7]%. At low SNRs, the improvement is small because the performance is dominated by the AWGN, while at high SNRs the improvement is significant because the performance is dominated by fading.
3) For the FU, increasing p_N from 0.1 to 0.2 increases interference, and thus the number of packets initially dropped increases, and the impact of RSIC also increases

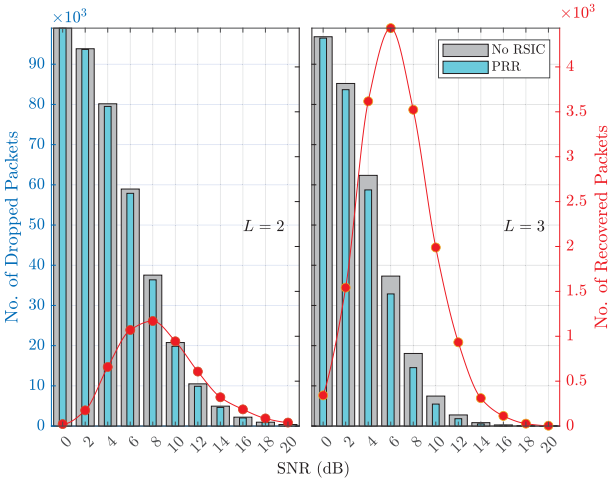

Fig. 10. Number of dropped and recovered packets for $\gamma_{\text{TN}} = 50$ dB at the NU receiver with $p_N = 0.1$.

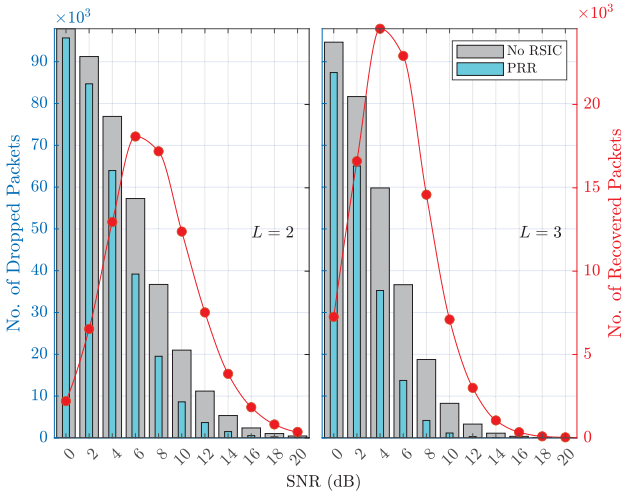

Fig. 11. Number of dropped and recovered packets for $\gamma_{\text{TN}} = 0$ dB at the FU receiver with $p_N = 0.1$.

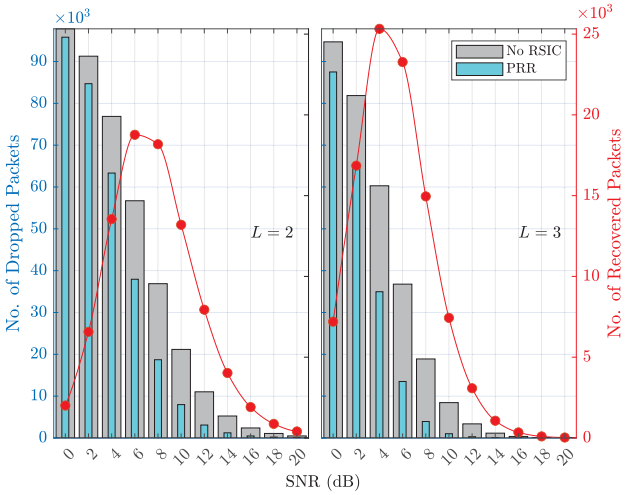

Fig. 12. Number of dropped and recovered packets for $\gamma_{\text{TN}} = 50$ dB at the FU receiver with $p_N = 0.1$.

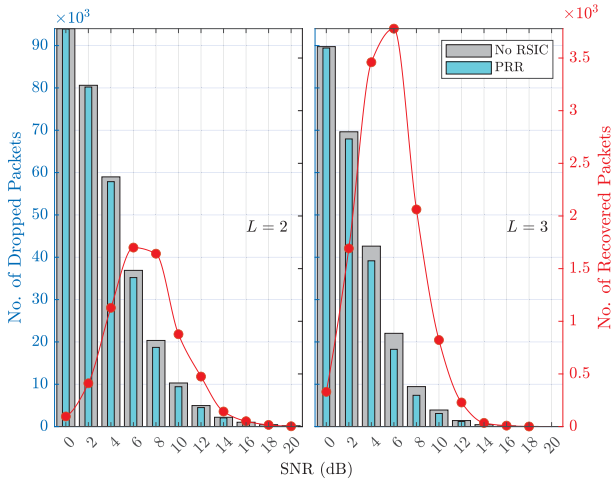

Fig. 13. Number of dropped and recovered packets for $\gamma_{\text{TN}} = 0$ dB at the NU receiver with $p_N = 0.2$.

due to its ability to mitigate interference. For example, comparing Figs. 11 and 15 for $L = 2$ shows that the number of packets initially dropped at SNR of 6 dB is 57 270 with $p_N = 0.1$ while it is 76 650 for $p_N = 0.2$. The number of recovered packets is 18 080 and 23 720 for $p_N = 0.1$ and $p_N = 0.2$, respectively.

4) The impact of the RSIC at the NU is generally smaller than that at the FU. This behavior is obtained because the FU packets at the NU can be detected mostly correctly due to their high power and strong channel of the NU. Therefore, canceling the interference from the FU would provide a marginal advantage. For example, when $p_N = 0.1$, SNR $= 6$ dB, and $L = 3$ in Fig. 10, the maximum number of recovered packets is 4 420, which corresponds to about 11.8% of dropped packets without RSIC. For the same settings, but with $p_N = 0.2$ as in Fig. 14, the RSIC managed to recover 8 190 packets out of 21 850 dropped packets, i.e., 37.4%. Comparing such results to those of the FU in Table IV shows the significant difference between the two users.
5) For the NU, increasing p_N from 0.1 to 0.2 reduces the number of packets dropped due to the increased power. However, the increased NU power also increases the interference, which emphasizes the impact of RSIC. For example, considering Figs. 9 and 13 at SNR $= 6$ dB and $L = 3$ shows that the number of packets recovered with $p_N = 0.1$ is 1 817 while it is 3 770, that is, 207.4%. The same trend can be observed for $\gamma_{\text{TN}} = 50$ dB in Figs. 10 and 14.
6) The quality of the TN channel, indicated by γ_{TN}, consistently improves the number of packets recovered for both users. This is due to the recoveries obtained using C-RSIC. For example, it can be seen from Figs. 9 and 10 that the number of recovered packets for $L = 2$ at SNR of 4 dB is 501 packets with $\gamma_{\text{TN}} = 0$ dB, while it is 1170 packets with $\gamma_{\text{TN}} = 50$ dB. Therefore, increasing γ_{TN} resulted in an improvement in packet recovery by 233.5%.

Table IV presents the ratio of the recovered packets to the dropped packets at the FU without RSIC for $\gamma_{\text{TN}} \in$

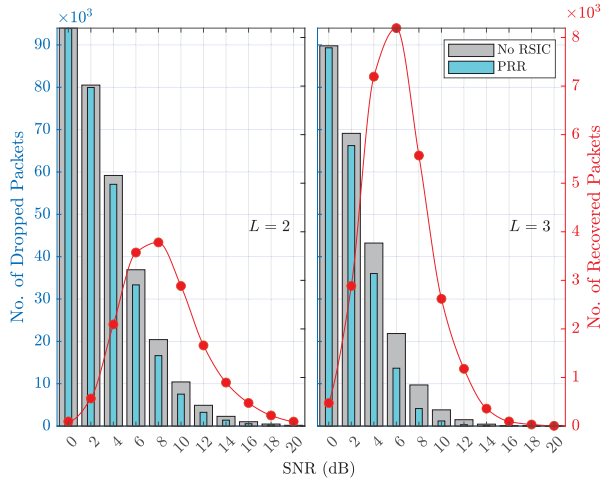

Fig. 14. Number of dropped and recovered packets for $\gamma_{\text{TN}} = 50$ dB at the NU receiver with $p_N = 0.2$.

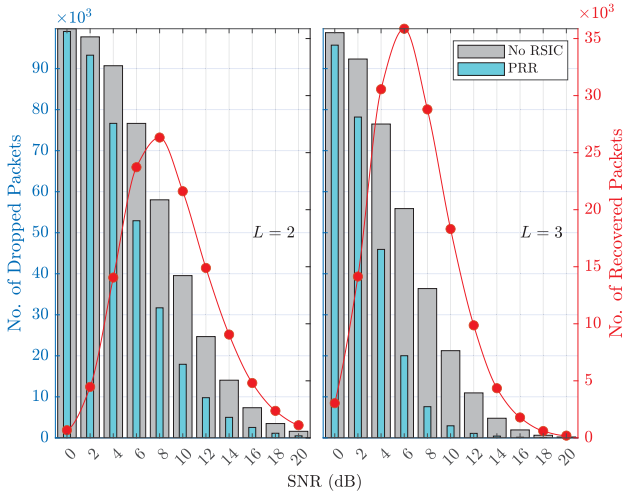

Fig. 15. Number of dropped and recovered packets for $\gamma_{\text{TN}} = 0$ dB at the FU receiver with $p_N = 0.2$.

$\{0, 50\}$ dB and $p_N \in \{0.1, 0.2\}$ with $L = 3$. As can be seen from the table, the RSIC has limited recovery capability at low SNRs because the performance is dominated by AWGN rather than interference. At high SNRs, the RSIC efficiency increases substantially. The improvement when $\gamma_{\text{TN}} = 0$ dB is achieved primarily using L-RSIC. Interestingly, the results using $\gamma_{\text{TN}} = 0$ and 50 dB are equivalent, while for $p_N = 0.2$ the improvement is significant when $\gamma_{\text{TN}} = 50$ dB where the C-RSIC contributes to the recovery process.

The proposed system is further evaluated in terms of throughput attained by both users. The throughput is defined as the ratio of correctly delivered packets $\bar{N}$ to the total number of transmitted/retransmitted packets T, i.e., Throughput $= (\bar{N}/T)$. Fig. 17 shows the results of the throughput achieved for $\gamma_{\text{TN}} = 50$ dB, $p_N = 0.2$, and $L = 3$. As can be seen in the figure, the throughput at high SNRs approaches one, which implies that no packets were dropped and no retransmissions were made. When the offline recovery process is activated after the asynchronous NOMA, no (re)transmissions occur. This means that T remains constant during the offline recovery process. The proposed scheme repairs and recovers packets dropped during asynchronous NOMA transmissions, thereby increasing $\bar{N}$. Consequently, $\bar{N}$ will either increase or remain the same after the start of the offline repair and recovery process. The throughput for NU is nearly the same for both

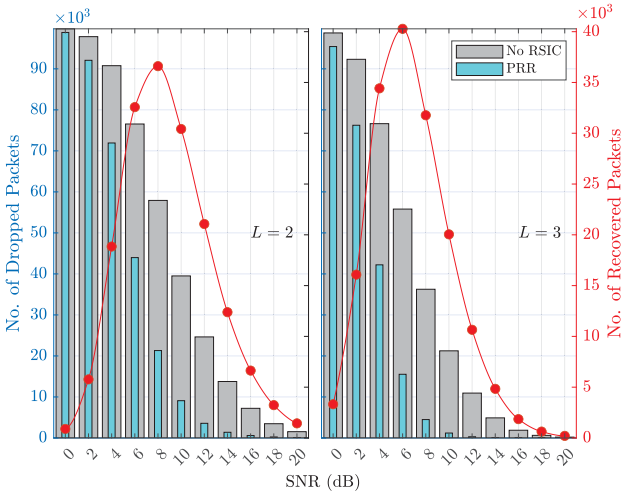

Fig. 16. Number of dropped and recovered packets for $\gamma_{\text{TN}} = 50$ dB at the FU receiver with $p_N = 0.2$.

TABLE IV
RECOVERED PACKETS RATIO (%) FOR THE FU, $L = 3$

SNR (dB)	$\gamma_{TN} = 0$ dB		$\gamma_{TN} = 50$ dB	
	$p_N = 0.1$	$p_N = 0.2$	$p_N = 0.1$	$p_N = 0.2$
0	7.6	3.0	7.6	3.3
2	20.3	15.3	20.5	17.4
4	41.0	39.9	42.1	44.9
6	62.5	64.1	63.2	72.1
8	77.8	79.1	79.2	87.6
10	85.9	86.1	87.9	94.3
12	91.0	90	91.3	97.3
14	93.6	92.3	92.9	98.7
16	93.1	92.3	94.2	98.5

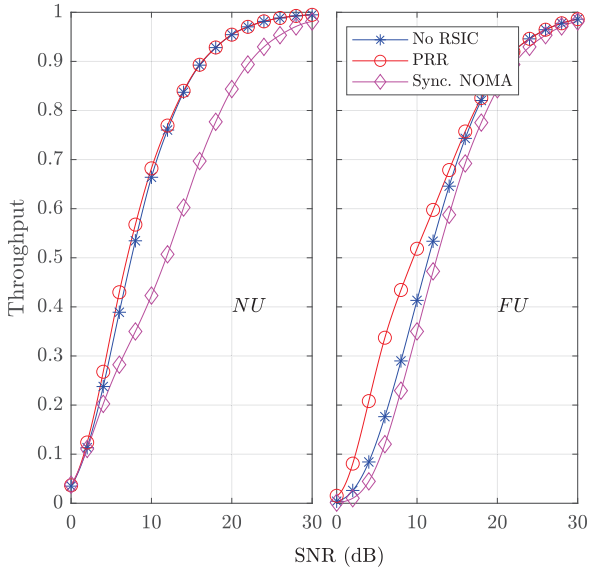

Fig. 17. Throughput achieved by the proposed asynchronous transmission compared to [65] for $p_N = 0.2$, $\gamma_{\text{TN}} = 50$ dB, and $L = 3$.

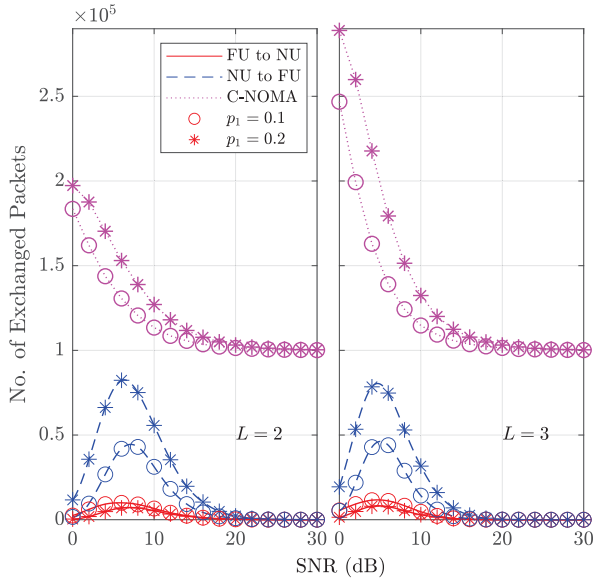

Fig. 18. Number of exchanged packets in the proposed NOMA with PRR and conventional C-NOMA for $\gamma_{\text{TN}} = 50$ dB.

cases. This is because the NU is recovering a few packets. The FU experiences a significant improvement in throughput up to 12 dB SNR. After 12 dB, both the PRR and no RSIC show nearly the same performance. In general, the NU outperforms FU in terms of throughput.

To evaluate the impact of the proposed asynchronous NOMA on throughput, it is compared to synchronous NOMA [65]. In synchronous NOMA, the LEOS sends new packets to the near- and FU only if it receives positive acknowledgments from both users, or when the current packets avail the maximum allowable transmissions. This approach ensures that the indices of both supercoded packets are always identical. It is evident that the proposed system substantially outperforms synchronous NOMA. The degradation of synchronous NOMA is due to the fact that even when one of the users correctly detects its own packet, it will still receive the same packet if the other user packet detection fails.

The overhead due to bidirectional cooperation in the proposed scheme is reported in terms of the number of packets exchanged between users, and it is compared to C-NOMA as shown in Fig. 18. Overhead results are presented for $\gamma_{\text{TN}} = 50$ dB. In C-NOMA, the NU detects and forwards the FU packet in each TS regardless of SNR. Therefore, the total number of exchanged packets is lower bounded by M and upper bounded by LM. Unlike C-NOMA, the RSIC overhead is significantly smaller, lower bounded by 0, and upper bounded by M. Such performance is achieved because the exchange process is dynamic, where it depends on the packet detection status at both users. At low SNRs, the number of exchanged packets is very small because both users will not be able to detect their own packets and hence will not request the exchange of any packet. In the mid range of SNRs, the number of packets exchanged peaks for both users $\forall p_N$. In this range, both users would have a sufficient number of correctly detected packets, and hence mutual cooperation would be beneficial for both users. At high SNRs, the number of exchanged packets is negligible because the recovery process is mostly carried out by the L-RSIC. It is also worth noting that the NU requests packets less frequently than the FU because the FU packets will be detected mostly correctly and stored in $\mathbb{A}_N$.

VI. Conclusion

In this article, we proposed a new PRR scheme for ARQ assisted NOMA communications in the context of IoT-LEOS networks. The proposed PRR is composed of three main elements, asynchronous ARQ-NOMA, bidirectional cooperative communications between the ground users, and offline packet repair using RSIC. The proposed schemes aims at maximizing the data that can be downloaded from the LEOS to the ground users during each flyover. The obtained results showed that asynchronous transmission can improve the throughput by decoupling the transmission of data packets from the two users. Moreover, the RSIC, local and cooperative, managed to reduce the mutual interference between the users and hence allow the recovery of several dropped packets. In certain scenarios, the proposed PRR managed to recover more than 90% of the packets that were initially dropped.

References

[1] W. Saad, M. Bennis, and M. Chen, "A vision of 6G wireless systems: Applications, trends, technologies, and open research problems," *IEEE Netw.*, vol. 34, no. 3, pp. 134–142, May/Jun. 2020.

[2] S. Dang, O. Amin, B. Shihada, and M.-S. Alouini, "What should 6G be?" *Nat. Electron.*, vol. 3, no. 1, pp. 20–29, 2020.

[3] (Ericsson, Stockholm, Sweden). *Ericsson Mobility Report, Q2 Update*, Aug. 2021. [Online]. Available: https://www.ericsson.com/en/mobility-report

[4] "Cisco annual Internet report (2018–2023)," Cisco, San Jose, CA, USA, Rep. C11-741490-01, 2020. [Online]. Available: https://www.cisco.com/c/en/us/solutions/collateral/executive-perspectives/annual-internet-report/white-paper-c11-741490.pdf.

[5] F. Zhao et al., (Commun. HUAWEI Res., Shenzhen, China). *Very-Low-Earth-Orbit Satellite Networks for 6G*, pp. 40–53, Sep. 2022, Accessed: Jan. 09, 2016. [Online]. Available: https://www.huawei.com/en/huaweitech/future-technologies/very-low-earth-orbit-satellite-networks-6g

[6] D. Nguyen et al., "6G Internet of Things: A comprehensive survey," *IEEE Internet Things J.*, vol. 9, no. 1, pp. 359–383, Jan. 2021.

[7] A. Benjebbour, K. Saito, A. Li, Y. Kishiyama, and T. Nakamura, "Non-orthogonal multiple access (NOMA): Concept, performance evaluation and experimental trials," in *Proc. Int. Conf. Wireless Netw. Mobile Commun. (WINCOM)*, Marrakech, Morocco, 2016, pp. 1–6.

[8] Z. Ding et al., "Application of non-orthogonal multiple access in LTE and 5G networks," *IEEE Commun. Mag.*, vol. 55, no. 2, pp. 185–191, Feb. 2017.

[9] M. Vaezi, R. Schober, Z. Ding, and H. V. Poor, "Non-orthogonal multiple access: Common myths and critical questions," *IEEE Wireless Commun.*, vol. 26, no. 5, pp. 174–180, Oct. 2019.

[10] O. Maraqa, A. S. Rajasekaran, S. Al-Ahmadi, H. Yanikomeroglu, and S. M. Sait, "A survey of rate-optimal power domain NOMA with enabling technologies of future wireless networks," *IEEE Commun. Surveys Tuts.*, vol. 22, no. 4, pp. 2192–2235, 4th Quart., 2020.

[11] L. Dai, B. Wang, Z. Ding, Z. Wang, S. Chen, and L. Hanzo, "A survey of non-orthogonal multiple access for 5G," *IEEE Commun. Surveys Tuts.*, vol. 20, no. 3, pp. 2294–2323, 3rd Quart., 2018.

[12] Y. Liu, Z. Qin, M. Elkashlan, Z. Ding, A. Nallanathan, and L. Hanzo, "Nonorthogonal multiple access for 5G and beyond," *Proc. IEEE*, vol. 105, no. 12, pp. 2347–2381, Dec. 2017.

[13] Z. Xiang, W. Yang, Y. Cai, Z. Ding, Y. Song, and Y. Zou, "NOMA-assisted secure short-packet communications in IoT," *IEEE Wireless Commun.*, vol. 27, no. 4, pp. 8–15, Aug. 2020.

[14] A. I. Perez-Neira, M. Caus, and M. A. Vazquez, "Non-orthogonal transmission techniques for multibeam satellite systems," *IEEE Commun. Mag.*, vol. 57, no. 12, pp. 58–63, Dec. 2019.

[15] Y. Liu, Z. Qin, Y. Cai, Y. Gao, G. Y. Li, and A. Nallanathan, "UAV communications based on non-orthogonal multiple access," *IEEE Wireless Commun.*, vol. 26, no. 1, pp. 52–57, Feb. 2019.

[16] H. Marshoud, P. C. Sofotasios, S. Muhaidat, G. K. Karagiannidis, and B. S. Sharif, "On the performance of visible light communication systems with non-orthogonal multiple access," *IEEE Trans. Wireless Commun.*, vol. 16, no. 10, pp. 6350–6364, Oct. 2017.

[17] M. Jain, N. Sharma, A. Gupta, D. Rawal, and P. Garg, "Performance analysis of NOMA assisted underwater visible light communication system," *IEEE Wireless Commun. Lett.*, vol. 9, no. 8, pp. 1291–1294, Aug. 2020.

[18] Y. Iraqi and A. Al-Dweik, "Power allocation for reliable SIC detection of rectangular QAM-based NOMA systems," *IEEE Trans. Veh. Technol.*, vol. 70, no. 8, pp. 8355–8360, Aug. 2021.

[19] *3GPP Series of Specifications: Evolved Universal Terrestrial Radio Access (E-UTRA)*, 3GPP Standard TS 36.101, Accessed: Jun. 14, 2020. [Online]. Available: https://www.3gpp.org/ftp/Specs/html-info/36-series.htm

[20] "Evolved universal terrestrial radio access (E-UTRA); radio link control (RLC) protocol specification (Release 15), Version 15.3.0.," 3GPP, Sophia Antipolis, France, Rep. TS 36.322, Sep. 2019, [Online]. Available: https://portal.3gpp.org/desktopmodules/Specifications/SpecificationDetails.aspx?specificationId=2438

[21] "Evolved universal terrestrial radio access (E-UTRA); medium access control (MAC) protocol specification (Release 8), Version 16.0.0.," 3GPP, Sophia Antipolis, France, Rep. TS 36.321, Apr. 2020, [Online]. Available: https://portal.3gpp.org/desktopmodules/Specifications/SpecificationDetails.aspx?specificationId=2437

[22] "Evolved universal terrestrial radio access (E-UTRA); physical layer procedures (Release 14), Version 16.0.0.," 3GPP, Sophia Antipolis, France, Rep. TS 36.213, Apr. 2020, [Online]. Available: https://portal.3gpp.org/desktopmodules/Specifications/SpecificationDetails.aspx?specificationId=2427

[23] *IEEE Standard for Information Technology—Telecommunications and Information Exchange Between Systems Local and Metropolitan Area Networks—Specific Requirements-Part-11: Wireless LAN Medium Access Control (MAC) and Physical Layer (PHY) Specifications*, Standard 802.11-2016, (Revision of IEEE Std 802.11-2012), Dec. 2016.

[24] Core specification, "Bluetooth special interest group," Bluetooth SIG, Kirkland, WA, USA, Rep. TS 5.2, 2019. [Online]. Available: https://www.bluetooth.org/docman/handlers/downloaddoc.ashx?doc_id=478726

[25] *IEEE Standard for Low-Rate Wireless Networks*, Standard 802.15.4-2020, (Revision of IEEE Std 802.15.4-2015), Aug. 2020.

[26] C. Chieler et al., "200 Gbps TBIRD CubeSat downlink: Preflight test results," in *Proc. 34th Free-Space Laser Commun.*, 2022, pp. 200–206.

[27] A. Flizikowski, T. Marciniak, T. A. Wysocki, and O. Oyerinde, "Selected aspects of non orthogonal multiple access for future wireless communications," *Math. Comput. Sci.*, vol. 17, no. 2, p. 10, 2023.

[28] A. Ahmed, A. Al-Dweik, Y. Iraqi, H. Mukhtar, M. Naeem, and E. Hossain, "Hybrid automatic repeat request (HARQ) in wireless communications systems and standards: A contemporary survey," *IEEE Commun. Surveys Tuts.*, vol. 23, no. 4, pp. 2711–2752, 4th Quart., 2021.

[29] X. Zhang, D. Guo, K. An, G. Zheng, S. Chatzinotas, and B. Zhang, "Auction-based multichannel cooperative spectrum sharing in hybrid satellite-terrestrial IoT networks," *IEEE Internet Things J.*, vol. 8, no. 8, pp. 7009–7023, Apr. 2021.

[30] A.-T. Le, N.-D. X. Ha, D.-T. Do, S. Yadav, and B. M. Lee, "Enabling NOMA in overlay spectrum sharing in hybrid satellite-terrestrial systems," *IEEE Access*, vol. 9, pp. 56616–56629, 2021.

[31] J. Li, K. Xue, D. S. L. Wei, J. Liu, and Y. Zhang, "Energy efficiency and traffic offloading optimization in integrated satellite/terrestrial radio access networks," *IEEE Trans. Wireless Commun.*, vol. 19, no. 4, pp. 2367–2381, Apr. 2020.

[32] N.-T. Nguyen, H.-N. Nguyen, N.-L. Nguyen, A.-T. Le, D.-T. Do, and M. Voznak, "Enhancing spectrum efficiency for multiple users in hybrid satellite-terrestrial networks," *IEEE Access*, vol. 9, pp. 50291–50300, 2021.

[33] V. Singh and P. K. Upadhyay, "Exploiting FD/HD cooperative-NOMA in underlay cognitive hybrid satellite-terrestrial networks," *IEEE Trans. Cogn. Commun. Netw.*, vol. 8, no. 1, pp. 246–262, Mar. 2022.

[34] M. Karavolos, N. Nomikos, D. Vouyioukas, and P. T. Mathiopoulos, "HST-NNC: A novel hybrid satellite-terrestrial communication with NOMA and network coding systems," *IEEE Open J. Commun. Soc.*, vol. 2, pp. 887–898, 2021.

[35] X. Yan, H. Xiao, K. An, G. Zheng, and W. Tao, "Hybrid satellite terrestrial relay networks with cooperative non-orthogonal multiple access," *IEEE Commun. Lett.*, vol. 22, no. 5, pp. 978–981, May 2018.

[36] F. Zhao, W. Xu, and W. Xiang, "Integrated satellite-terrestrial networks with coordinated C-NOMA and relay transmission," *IEEE Syst. J.*, vol. 16, no. 4, pp. 5270–5280, Dec. 2022.

[37] L. Han, W.-P. Zhu, and M. Lin, "Outage analysis of multi-relay NOMA-based hybrid satellite-terrestrial relay networks," *IEEE Trans. Veh. Technol.*, vol. 71, no. 6, pp. 6469–6487, Jun. 2022.

[38] L. Han, W.-P. Zhu, and M. Lin, "Outage analysis of NOMA-based multiple-antenna hybrid satellite-terrestrial relay networks," *IEEE Commun. Lett.*, vol. 25, no. 4, pp. 1109–1113, Apr. 2021.

[39] X. Tang, K. An, K. Guo, Y. Huang, and S. Wang, "Outage analysis of non-orthogonal multiple access-based integrated satellite-terrestrial relay networks with hardware impairments," *IEEE Access*, vol. 7, pp. 141258–141267, 2019.

[40] L. Han, W.-P. Zhu, and M. Lin, "Outage of NOMA-based hybrid satellite-terrestrial multi-antenna DF relay networks," *IEEE Wireless Commun. Lett.*, vol. 10, no. 5, pp. 1083–1087, May 2021.

[41] X. Yan, H. Xiao, C.-X. Wang, and K. An, "Outage performance of NOMA-based hybrid satellite-terrestrial relay networks," *IEEE Wireless Commun. Lett.*, vol. 7, no. 4, pp. 538–541, Aug. 2018.

[42] X. Li, Y. Chen, P. Xue, G. Lv, and M. Shu, "Outage performance for satellite-assisted cooperative NOMA systems with coordinated direct and relay transmission," *IEEE Commun. Lett.*, vol. 24, no. 10, pp. 2285–2289, Oct. 2020.

[43] B. Zhao, G. Ren, and X. Dong, "Joint NOMA clustering and power allocation in IoRT-oriented satellite terrestrial relay networks," *IEEE Trans. Veh. Technol.*, vol. 71, no. 10, pp. 11078–11088, Oct. 2022.

[44] N. Wang, F. Li, D. Chen, L. Liu, and Z. Bao, "NOMA-based energy-efficiency optimization for UAV enabled space-air-ground integrated relay networks," *IEEE Trans. Veh. Technol.*, vol. 71, no. 4, pp. 4129–4141, Apr. 2022.

[45] H. Shuai, K. Guo, K. An, and S. Zhu, "NOMA-based integrated satellite terrestrial networks with relay selection and imperfect SIC," *IEEE Access*, vol. 9, pp. 111346–111357, 2021.

[46] R. Liu, K. Guo, K. An, S. Zhu, and H. Shuai, "NOMA-based integrated satellite-terrestrial relay networks under spectrum sharing environment," *IEEE Wireless Commun. Lett.*, vol. 10, no. 6, pp. 1266–1270, Jun. 2021.

[47] R. Liu, K. Guo, K. An, and S. Zhu, "NOMA-based overlay cognitive integrated satellite-terrestrial relay networks with secondary network selection," *IEEE Trans. Veh. Technol.*, vol. 71, no. 2, pp. 2187–2192, Feb. 2022.

[48] N.-L. Nguyen, H.-N. Nguyen, A.-T. Le, D.-T. Do, and M. Voznak, "On performance analysis of NOMA-aided hybrid satellite terrestrial relay with application in small-cell network," *IEEE Access*, vol. 8, pp. 188526–188537, 2020.

[49] X. Zhang et al., "On the performance of hybrid satellite-terrestrial content delivery networks with non-orthogonal multiple access," *IEEE Wireless Commun. Lett.*, vol. 10, no. 3, pp. 454–458, Mar. 2021.

[50] M. Toka, M. Vaezi, and W. Shin, "Outage analysis of Alamouti-NOMA scheme for hybrid satellite–terrestrial relay networks," *IEEE Internet Things J.*, vol. 10, no. 6, pp. 5293–5303, Mar. 2023.

[51] K. An, M. Lin, J. Ouyang, and W.-P. Zhu, "Secure transmission in cognitive satellite terrestrial networks," *IEEE J. Sel. Areas Commun.*, vol. 34, no. 11, pp. 3025–3037, Nov. 2016.

[52] Z. Lin et al., "Refracting RIS-aided hybrid satellite-terrestrial relay networks: Joint beamforming design and optimization," *IEEE Trans. Aerosp. Electron. Syst.*, vol. 58, no. 4, pp. 3717–3724, Aug. 2022.

[53] Z. Lin, M. Lin, B. Champagne, W.-P. Zhu, and N. Al-Dhahir, "Secrecy-energy efficient hybrid beamforming for satellite-terrestrial integrated networks," *IEEE Trans. Commun.*, vol. 69, no. 9, pp. 6345–6360, Sep. 2021.

[54] Z. Lin, M. Lin, T. de Cola, J.-B. Wang, W.-P. Zhu, and J. Cheng, "Supporting IoT with rate-splitting multiple access in satellite and aerial-integrated networks," *IEEE Internet Things J.*, vol. 8, no. 14, pp. 11123–11134, Jul. 2021.

[55] Z. Xiao et al., "LEO satellite access network (LEO-SAN) towards 6G: Challenges and approaches," 2022, *arXiv:2207.11896*. [Online]. Available: https://arxiv.org/abs/2207.11896

[56] I. Dias, L. Ruan, C. Ranaweera, and E. Wong, "From 5G to beyond: Passive optical network and multi-access edge computing integration for latency-sensitive applications," *Opt. Fiber Technol.*, vol. 75, Jan. 2023, Art. no. 103191.

[57] T. Waliwander and C. Farran. "THz–to be or not to be in 6G?" Accessed: Feb. 12, 2023. [Online]. Available: https://www.microwavejournal.com/articles/print/38119-thz-to-be-or-not-to-be-in-6g

[58] "Telesat lightspeed: The world's most advanced LEO constellation." Accessed: Feb. 12, 2023. [Online]. Available: https://www.telesat.com/wp-content/uploads/2022/05/Telesat-Lightspeed-Resiliency.pdf
[59] G. M. Capez, S. Henn, J. A. Fraire, and R. Garello, "Sparse satellite constellation design for global and regional direct-to-satellite IoT services," *IEEE Trans. Aerosp. Electron. Syst.*, vol. 58, no. 5, pp. 3786–3801, Oct. 2022.
[60] J. Chu, X. Chen, C. Zhong, and Z. Zhang, "Robust design for NOMA-based multibeam LEO satellite Internet of Things," *IEEE Internet Things J.*, vol. 8, no. 3, pp. 1959–1970, Feb. 2020.
[61] X. Yan et al., "The application of power-domain non-orthogonal multiple access in satellite communication networks," *IEEE Access*, vol. 7, pp. 63531–63539, 2019.
[62] A. Abdi, W. Lau, M.-S. Alouini, and M. Kaveh, "A new simple model for land mobile satellite channels: First-and second-order statistics," *IEEE Trans. Wireless Commun.*, vol. 2, no. 3, pp. 519–528, May 2003.
[63] L. Yang and M. O. Hasna, "Performance analysis of amplify-and-forward hybrid satellite-terrestrial networks with cochannel interference," *IEEE Trans. Commun.*, vol. 63, no. 12, pp. 5052–5061, Dec. 2015.
[64] Z. Zhang et al., "User activity detection and channel estimation for grant-free random access in LEO satellite-enabled Internet of Things," *IEEE Internet Things J.*, vol. 7, no. 9, pp. 8811–8825, Sep. 2020.
[65] D. Cai, Z. Ding, P. Fan, and Z. Yang, "On the performance of NOMA with hybrid ARQ," *IEEE Trans. Veh. Technol.*, vol. 67, no. 10, pp. 10033–10038, Oct. 2018.

Ashfaq Ahmed (Senior Member, IEEE) received the M.S. and Ph.D. degrees from the Department of Electronics and Telecommunications, Politecnico di Torino, Torino, Italy, in 2010 and 2014, respectively.

He is currently affiliated with the Center for Cyber-Physical Systems, Department of Computer and Communication Engineering, Khalifa University, Abu Dhabi, UAE. He was an Assistant Professor with the Department of Electrical and Computer Engineering, COMSATS University Islamabad, Wah Campus, Rawalpindi, Pakistan, from March 2014 to March 2021. He has hands-on experience with simulation and modeling of optimization problems, as well as working with a variety of optimization toolboxes, including the MATLAB optimization toolbox and the OPTI toolbox. He also developed heuristics and applied several meta-heuristics to various optimization problems. His research interests include hardware security, security protocols, computational intelligence, evolutionary algorithms, convex optimization, resource allocation, and applied optimization for 5G and beyond 5G applications, cloud computing, and physical-layer wireless communication.

Arafat Al-Dweik (Senior Member, IEEE) received the M.S. (Summa Cum Laude) and Ph.D. (Magna Cum Laude) degrees in electrical engineering from Cleveland State University, Cleveland, OH, USA, in 1998 and 2001, respectively.

He is currently with the Department of Computer and Communication Engineering, Khalifa University, Abu Dhabi, UAE. He was also with Efficient Channel Coding Inc., Cleveland, OH, USA; the Department of Information Technology, Arab American University, Jenin, Palestine; and the University of Guelph, Guelph, ON, Canada. He is a Visiting Research Fellow with the School of Electrical, Electronic, and Computer Engineering, Newcastle University, Newcastle upon Tyne, U.K., and a Research Professor with Western University, London, ON, Canada, and the University of Guelph. He has extensive research experience in various areas of wireless communications that include modulation techniques, channel modeling and characterization, synchronization and channel estimation techniques, OFDM technology, error detection and correction techniques, MIMO, and resource allocation for wireless networks.

Dr. Al-Dweik was the recipient of the Hijjawi Award for Applied Sciences in 2003, the Fulbright Alumni Development Grant in 2003 and 2005, the Dubai Award for Sustainable Transportation in 2016, and the UAE Leader-Founder Award in 2019. He was awarded the Fulbright Scholarship from 1997 to 1999. He serves as an Associate Editor for the IEEE TRANSACTIONS ON VEHICULAR TECHNOLOGY and the *IET Communications*. He is a Registered Professional Engineer in Ontario, Canada. He is a member of Tau Beta Pi and Eta Kappa Nu.

Youssef Iraqi (Senior Member, IEEE) received the M.Sc. and Ph.D. degrees in computer science from the University of Montreal, Montreal, QC, Canada, in 2000 and 2003, respectively.

He is currently an Associate Professor with the School of Computer Science, Mohammed VI Polytechnic University, Ben Guerir, Morocco. Before that, he was with the Department of Electrical Engineering and Computer Science, Khalifa University (KU), Abu Dhabi, UAE, for 12 years. Before joining KU, he was the Chair of the Department of Computer Science, Dhofar University, Salalah, Oman, for four years. From 2004 to 2005, he was a Research Assistant Professor with the David R. Cheriton School of Computer Science, University of Waterloo, Waterloo, ON, Canada. He has published more than 130 research papers in international journals and refereed conference proceedings. His research interests include resource management in wireless networks, blockchain, trust and reputation management, cloud computing, and stylometry.

Dr. Iraqi received the IEEE Communications Society Fred W. Ellersick Paper Award in the field of communications systems in 2008. He is on many technical program committees of international conferences and is always approached for his expertise by international journals in his field.

Ernesto Damiani (Senior Member, IEEE) received the Ph.D. degree in computer science from the University of Milan, Milan, Italy, in 1994.

He is currently a Full Professor with the Università degli Studi di Milano, Milan, Italy; and the Senior Director of the Robotics and Intelligent Systems Institute, and the Director of the Center for Cyber Physical Systems (C2PS), Khalifa University, Abu Dhabi, UAE. He is also the Leader of the Big Data Area with the Etisalat British Telecom Innovation Center and the President of the Consortium of Italian Computer Science Universities. He is also a part of the ENISA Ad-Hoc Working Group on Artificial Intelligence Cybersecurity. He has pioneered model-driven data analytics. He has authored more than 650 Scopus-indexed publications and several patents. His research interests include cyber–physical systems, big data analytics, edge/cloud security and performance, artificial intelligence, and machine learning.

Dr. Damiani was the recipient of the Research and Innovation Award from the IEEE Technical Committee on Homeland Security, the Stephen Yau Award from the Service Society, the Outstanding Contributions Award from IFIP TC2, the Chester-Sall Award from IEEE IES, the IEEE TCHS Research and Innovation Award, and the Doctorate Honoris Causa from INSA-Lyon, France, for his contribution to Big Data Teaching and Research.